Copy: Mr.& Mrs. S.C. Spiers
136 Henry St.,
Brantford, Ontario.

EXPERIMENTAL STUDY OF

RETURN FLOW HARBOUR RESONATORS

EXPERIMENTAL STUDY OF RETURN FLOW DRAWN FROM HARBOUR RESONATORS

By

TERRENCE G. SPIERS, B.ENG.

A Project

Submitted to the School of Graduate Studies

in Partial Fulfilment of the Requirements

for the Degree

Master of Engineering

McMaster University

April 1976

MASTER OF ENGINEERING (1976) McMASTER UNIVERSITY
(Civil) Hamilton, Ontario

TITLE: Experimental Study of Return Flow
Drawn from Harbour Resonators

AUTHOR: Terrence G. Spiers, B.Eng. (McMaster University)

SUPERVISOR: Doctor W.James

NUMBER OF PAGES: x , 90

ABSTRACT

This report describes an experimental investigation into the potential use of return flow from rectangular harbour resonators incorporated into semi-infinite harbour entrances. The mechanism studied includes: the bandwidth of the reduced energy spectrum transmitted into a harbour, the concomitant reflected wave spectra and the energy available for return flow. This report is intended to provide data for the design of on-channel harbour resonators so as to eliminate or reduce the transmission of a selected band of harmful wave frequencies and to maximize the energy of scouring currents so as to prevent the influx and deposition of littoral sediments in harbour entrances. Observations were also made of the potential danger to small vessels provided by the movement of waves into and out of the resonators. The vessels would probably be ejected from the resonator without risk of battering, although the motion locally in the mouth of the resonator will be amplified.

ACKNOWLEDGEMENTS

For their assistance in the preparation of this thesis, I would like to acknowledge the following:

The Department of Public Works of Canada for their financial assistance in development of testing facilities.

Dr. William James, my supervisor, for his guidance and encouragement throughout the study.

Mrs. Annie Spiers, my wife, for her diligence and hard work in both editing and preparing the manuscript.

My parents and family for their encouragement and support throughout my education.

TABLE OF CONTENTS

SYMBOLS

Notation - Lower Case

a_i	incident wave amplitude
a_r	reflected wave amplitude
a_t	transmitted wave amplitude
d	resonator length
g	gravitational constant = 32.2 ft/sec^2
h_c	main channel water depth
h_{rw}	resonator rear wall height
h_s	submerged depth of flap hinge
$\overline{h}_{sb}$	mean depth increase in overflow reservoir
k	wave number = $2\pi/\lambda$
w	resonator width
x	horiz. dist., in direction of wave propagation
y	vert. dist., with origin at surface

Notation - Upper Case

A_e	area of junction element = W·w
C	velocity of wave propagation (phase velocity)
C_G	wave group velocity
$\overline{E}_k$	average kinetic energy
E_L	(H_L) clapotis envelope antinode height
E_N	(H_N) clapotis envelope node height
$\overline{E}_p$	average potential energy
$\overline{E}_t$	transmitted wave energy
$\overline{E}_{to}$	total wave energy
H_i	incident wave height
H_r	reflected wave height
H_t	transmitted wave height
I_e	flow into junction element
L_f	length of overflow ramp

O_e	flow out of junction element
$\overline{P}_i$	average incident wave power
$\overline{P}_r$	average reflected wave power
$\overline{P}_{rf}$	average return flow power
$\overline{P}_t$	average transmitted wave power
$\overline{P}_{to}$	total wave power
$\overline{Q}_{rf}$	single resonator return flow discharge
SWL	still water level
T	wave period
W	main channel width

Notation - Subscripts

e	junction element
i	incident
r	reflected
rf	return flow
t	transmitted
to	total

Notation - Greek Letters - Lower Case

α	(alpha) coefficient of reflectivity
β	(beta) coefficient of transmissivity
γ	(gamma) specific weight of water = ρg
ε	(epsilon) overflow ramp angle to horizontal
η	(eta) vert.displacement from mean position
θ	(theta) power extraction coefficient
λ	(lambda) local wave length
μ	(mu) velocity in x-direction
ξ	(xi) horiz. displacement from mean position
π	(pi) = 3.1415926
ρ	(rho) density - mass per unit volume = γ/g
σ	(sigma) wave angular frequency = $2\pi/T$
υ	(upsilon) velocity in y-direction
ϕ	(phi) velocity potential function

FIGURES

INTRODUCTION

1.1 General Harbour Design

For as long as man has sailed ships he has required and built safe shelters for his vessels. Since most natural ports have now been developed, further expansion must turn to less desirable sites. For both natural and man-made harbours, the engineer must deal with a variety of problems before the harbour will function properly or economically.

Basically a harbour must serve as a shelter in adverse weather conditions and as an easily accessible port for loading and unloading cargo and passengers. The main design considerations in the construction of a harbour facility for use by either pleasure crafts or commercial vessels include provisions for:

a) manoeuvering space
b) easy approach
c) ample depths
d) instantaneous currents less than 3 knots
e) self-cleansing water circulation
f) a minimum of dredging and maintenance.

General rules-of-thumb design criteria are given by the A.S.C.E.[1] for entrances allowing simultaneous movement into and out of the harbour. The width should be 5 times the beam width of the largest vessel likely to use the facility; depths should be at least the sum of maximum draft, squat due to the vessel's speed, one half the maximum wave height plus a small additional depth for a margin of safety.

1.2 Traditional Harbour Entrance Structures and Wave Problems

In the past the provision of an easy approach has been difficult due to the limited methods available for preventing wave penetration into the harbour. These methods included conventional breakwaters, to dissipate and reflect the waves, and staggered or offset entrance channels, to isolate the harbour from reflected and diffracted waves. Jetties were also used in an attempt to prevent littoral sediments from encroaching upon and entering into the harbour entrance channel[1]. These jetties often caused more damage than they purported to prevent. A disruption of sediment transport along a coastal zone often results in extensive erosion along the down drift coastline and substantial accretion in the area immediately updrift of the jetty. Methods for bypassing of this material include sediment bypassing plants, pumping dredges and dragline dredges. Most authorities annually spend large amounts of money on these dredging or by-passing facilities. In tidal ports

it has been possible to use the fluctuations in water depth for periodic recharge of sluicing basins which provide small scour flows during ebb tides. According to Cornick[3], this small return flow helps prevent siltation and aids manoeuvering. Unfortunately , Cornick found that transmission of incident waves into the harbour domain was not significantly affected by the passage of these small currents.

1.3 Canadian Harbours with Resonators

Harbour resonators have recently been used in a number of Canadian harbours, both tidal and non-tidal. James[13] has demonstrated experimentally that these structures effectively reduce wave energy transmitted into the harbour, yet provide no restriction to shipping. On the contrary, a clear navigable channel is provided which requires little, if any, navigational manoeuvers. Resonators basically comprise a system of short rectangular branch canals completely enclosed on three sides, built orthogonally onto the entrance breakwaters of a harbour[13]. Valembois[25] was a pioneer in the use of these resonators and first proposed their operation in 1953. Their performance has been well studied in the interval between their conception and their use on real harbour situations. In Nova Scotia, the ports of Dingwall, Inverness and Pleasant Bay have resonant structures to improve harbour

entrance effectiveness.

The Dingwall harbour incorporates a special geometry for a battery of resonators, described by Donnelly and MacInnis[5] as a "limit" geometry. The simple triangular geometry shown in Figure 1-1, has the same general shape as a battery of numerous resonators of increasing depth as shown in Figure 1-2. This harbour, built in 1962, has reported a periodic self-flushing current which was inexplicable. A model study of this harbour by White[26] was unable to reproduce the periodic flushing action. White believed that this action was due to mass transport in the incident waves into the resonators due to their position of breaking relative to the harbour entrance. The self-scouring performance of this harbour has been unsatisfactory. The average depth of the main channel in 1962 was approximately 12 feet. Donnelly and MacInnis[5] found that even after extensive dredging the harbour is now silted to a depth of 5 feet during low tide. This is only marginally acceptable for the vessels using the port.

Prandle[22] studied the inland port of Kincardine which employes a single resonator to reduce inner harbour oscillations. It was reported that wave action in the vicinity of the resonators was troublesome but not as bad as previously recorded at resonant modes for the harbour. This might be exacerbated by the reduction in channel width caused by the location of the resonator wing-walls.

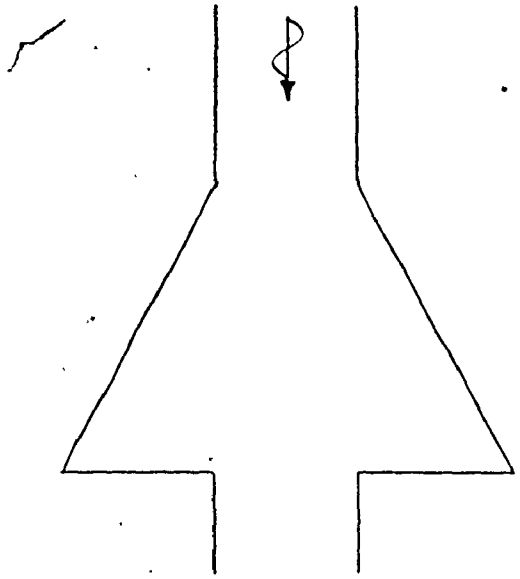

Fig. 1-1 : "Limit" Geometry

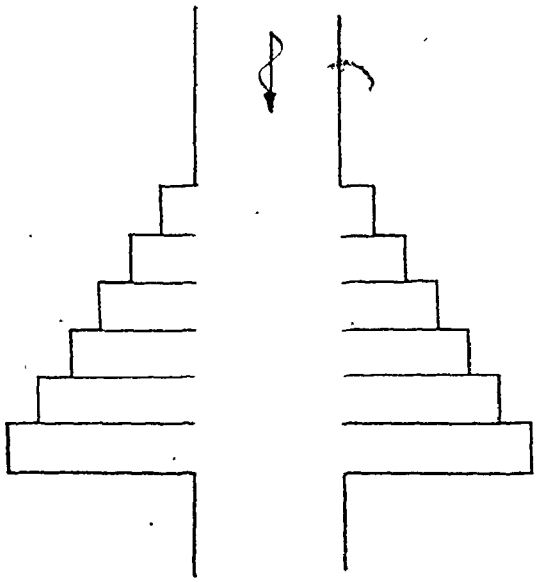

Fig. 1-2 : Resonator Battery

1.4 Introduction to Resonator Studies

The performance of rectangular resonators for various configurations, wave periods, entrance widths and water depths has been previously studied and documented. The theory describing their behaviour is based upon first order linear wave theory and the assumption of irrotational motion. A summary of the important findings regarding the behaviour of resonators illustrates the degree of development of this innovation.

James[11,12,13,14] carried out considerable work in this field and has developed numerous design methods and innovations for improving the performance of harbour resonators. The design curves reproduced in Figures 1-3 to 1-5, were developed to predict the performance of resonators for various geometries for the first resonant mode. The first and second resonant modes occur when the resonator acts as either a branch canal or expansion chamber respectively as shown in Figures 1-6 and 1-7. In these studies it was found that resonator performance was dependant on the actual size of the resonator chamber as well as the main channel width and the uniformity of water depth in the resonator and main entrance channel. James[13] found that resonator operation was acceptable provided that the main entrance channel width did not exceed the design wavelength of the resonator. This limitation seems to be the most restrictive in the potential use of resonators.

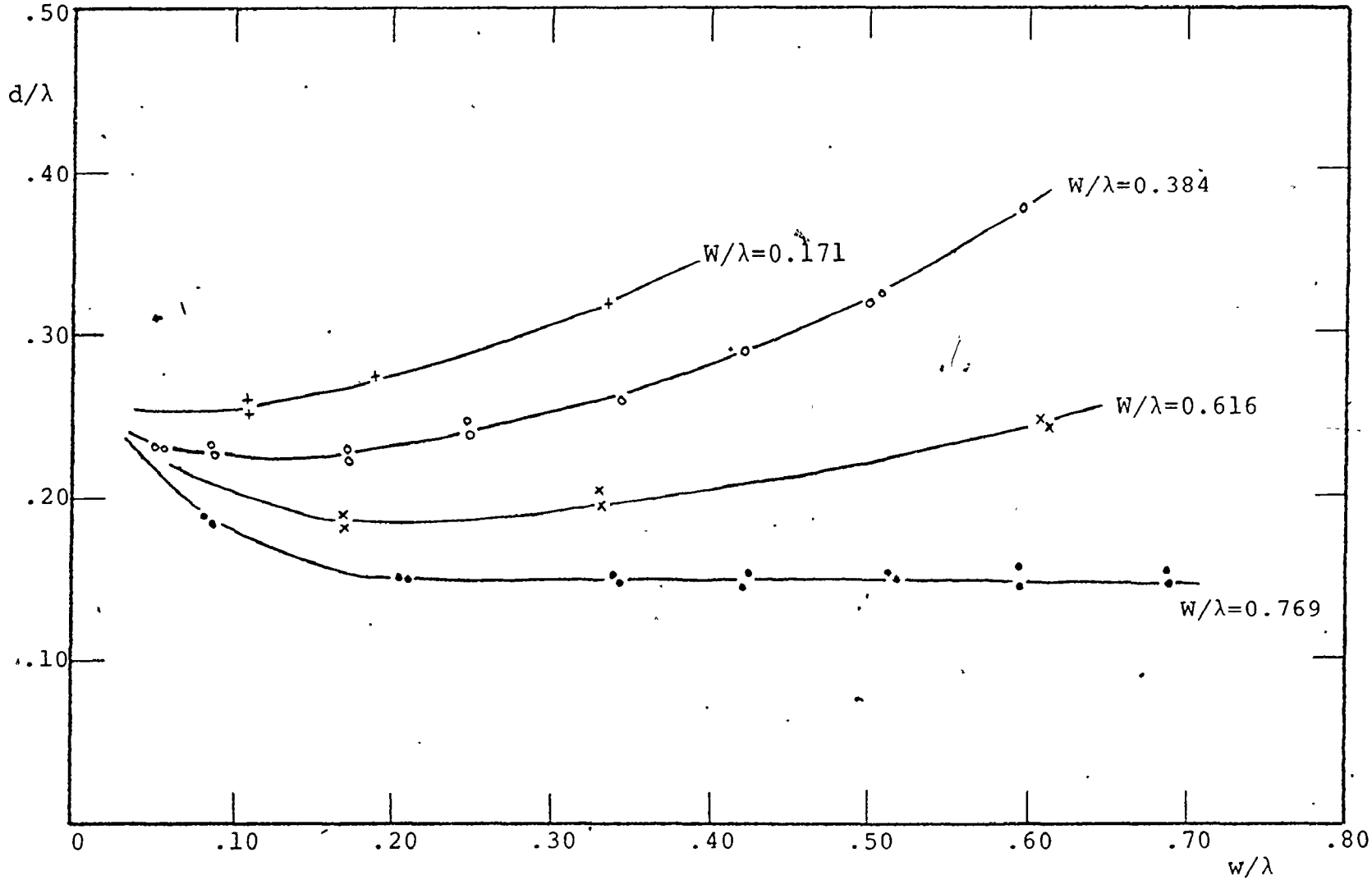

Figure 1-3 : Geometry for Resonance (mode 1)

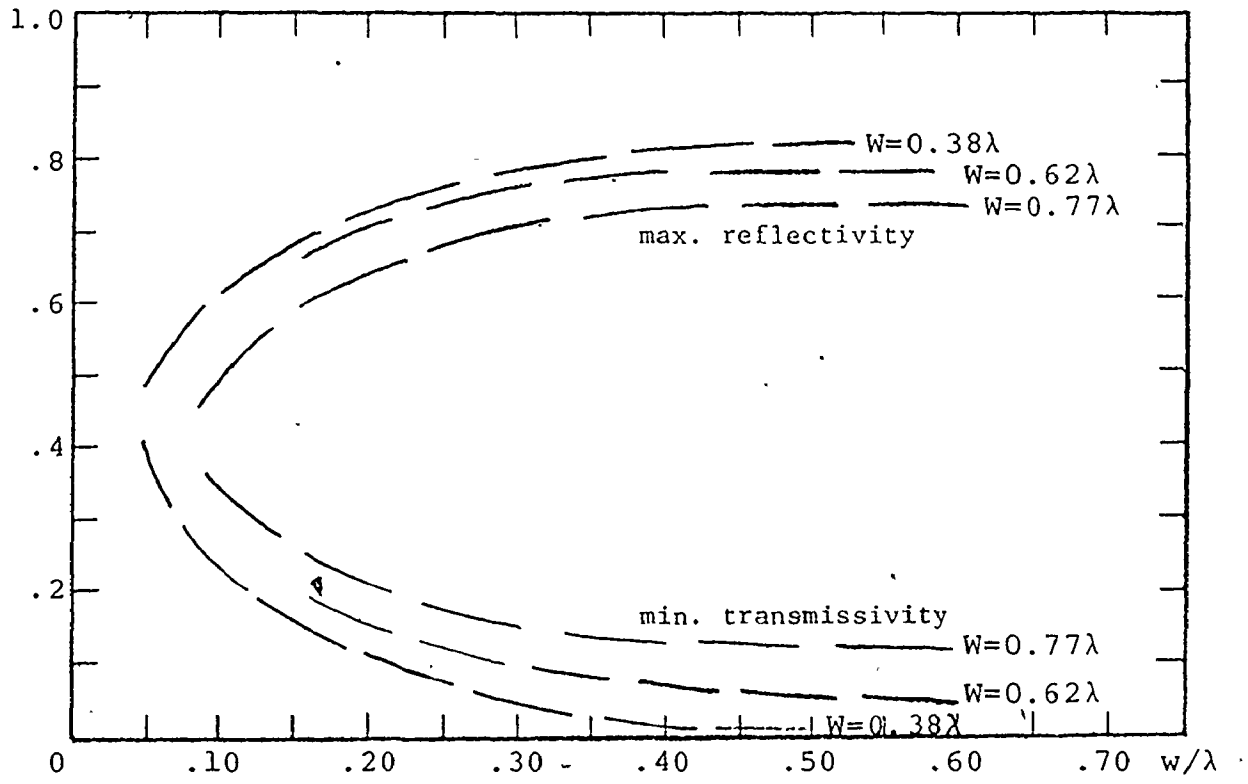

Fig. 1-4 : Resonant Maxima and Minima

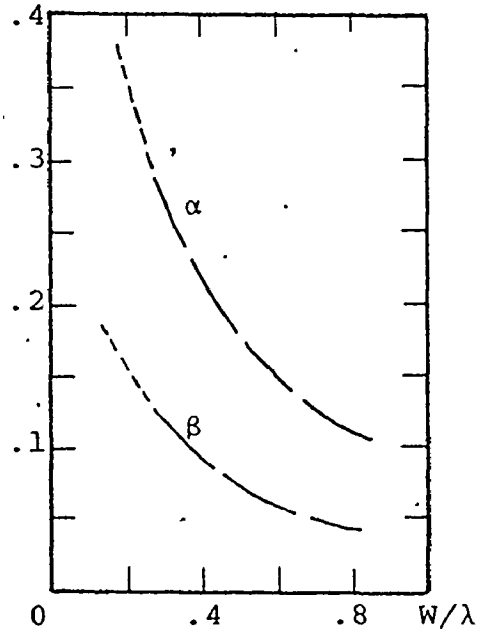

Fig. 1-5 : Tuning Parameter Bandwidth
at half resonant value

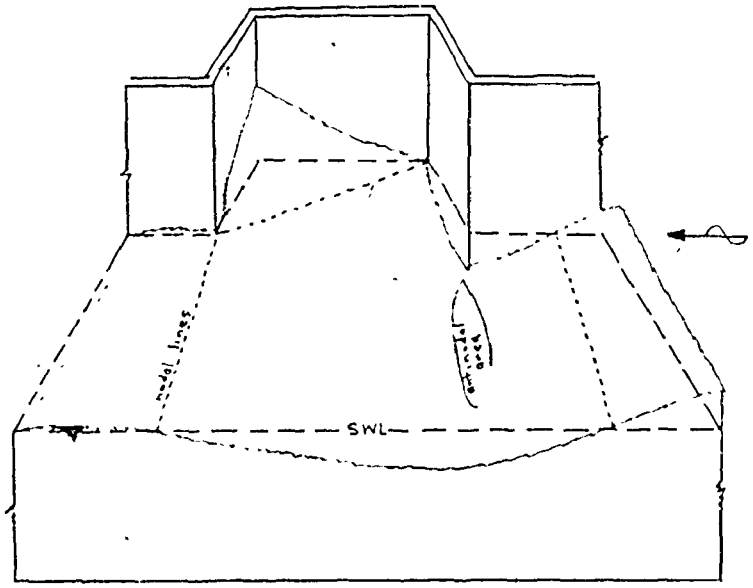

Fig. 1-6 : Mode 1

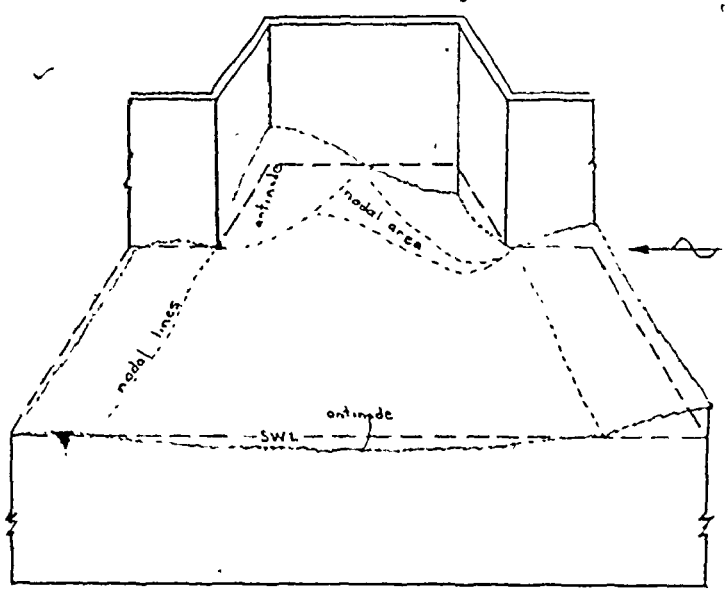

Fig. 1-7 : Mode 2

1.5 Innovations in Harbour Resonators

Resonator geometry for most efficient operation, as initially derived by Valembois, has depth "d" equal to 1/4 or 3/4 of the design wavelength and width "w" equal to 1/2 the design wavelength. We know now that these values are dependant on channel width "W" as shown in Fig. 1-3, and on uniformity of water depth in the resonator and main channel. In fact quarter-wavelength resonators can give anti-resonance with total transmission of the incident waves into the harbour. Still water depth "h_c" is of little or no consequence in the resonator geometry for resonance since the results are plotted in the ka plane. Non-uniform depths effectively reduce the performance and alter the response downward toward smaller frequencies according to James[11,13,17]. This could provide considerable savings in construction due to reduced excavation depths and resonator sizes, but at the expense of resonator efficiency, higher transmissivity and lower reflectivity. Smaller values of the resonator width parameter "w/λ", resulted in decreased efficiency and higher velocities in the resonator mouth[13]. This is also the condition for resonant mode 1. Resonant mode 2 will incur much smaller amplitudes and thus lower velocities in the resonator mouth. Thus this mode is safer for navigation. Incident wave amplitude affects energy losses and has little effect on the resonator geometry for resonance. Both transmissivity minima and

reflectivity maxima are amplitude dependant[14].

1.6 Spectral Response

Battery configurations are used to cover a broader band of incident wave frequencies. In this case the smallest resonator, that is the resonator tuned to the highest wave frequency, is usually placed nearest the ocean or incident wave domain, with larger resonators in ascending order downstream toward the harbour. The operation of such resonators in battery form has been shown to be approximately linear in that the effect of the battery is the sum of the effects of the independant resonators[17]. Resonator batteries operate most efficiently when they are not contiguous[11,17]. The triangular "limit" geometry, mentioned earlier, is not as effective as the same configuration with isolating resonator walls. The design curves presented in Figures 1-3 to 1-5 can be used to calculate the anticipated spectral response for the battery, but only for the first resonant mode. The spectral response can also be determined very effectively and quickly by using an acoustic model. Acoustic models used in this type of work showed no scale effects and provided quick and accurate response curves at very little cost[17].

1.7 Sediment Transport Aspects

Rectangular resonators, used either individually or

in battery form should be placed as near as possible to the ocean end of the entrance channel. This reduces the extent of the partial clapotis, caused by the superposition of the reflected waves on the incident waves, to a relatively short section of the entrance channel. The partial clapotis also helps to prevent influx of littoral sediments by reducing mass transport. The amplified orbital bed motion causes bed sediments to saltate; this suspension is transported by the second order mass transport or drift currents. In a series of tests, Lates[18] observed that by constructing a minimum of three resonators in a battery configuration, where main channel widths were limited to 0.7λ to λ, influx of littoral sediments was greatly reduced by the action of the reflected waves or partial clapotis in the channel mouth. Agitation in the harbour entrance discourages deposition of material and would obviously be an effective means of sediment by-passing.

1.8 Return Flow Resonators

The configuration tested in this report is a single pair of geometrically opposed rectangular resonators. The partial clapotis phenomena will provide the agitation required to keep the sediment in suspension while a new innovation; a return flow derived from overflow in the resonator basins, will prohibit the movement of this sediment into the harbour entrance. Cornick[3] gives the

typical return flow velocities required to move various classifications of sediment as listed in table 1.

TABLE 1

MATERIAL	CRITICAL VELOCITY
Silt,mud,very soft clays	3 in/sec.
Fine sand,loam	5 in/sec.
Ordinary clay	6 in/sec.
Coarse sand,fine gravel	7 in/sec.
Fairly coarse gravel	1 ft/sec.
Large shingle(1-1/2 in. pebbles)	3 ft/sec.

The return flow velocities in this study cannot be compared directly with these flows because of the effect of the amplified orbital velocities. However, general conclusions can be drawn as to whether this method will provide a plausible solution to the problems encountered in maintaining sediment-free harbour entrances.

THEORY

2.1 Notation

A definition sketch, together with the co-ordinate system used, is presented in Figure 2-1.

2.2 Relevant Results from Potential Theory[9]

Wave motion is assumed to have been generated from rest by normal forces and the resultant motion is thus irrotational. Hence there will be a velocity potential function ϕ such that the principle of conservation of mass can be expressed as:

$$\frac{\partial^2\phi}{\partial x^2} + \frac{\partial^2\phi}{\partial y^2} = 0 \qquad (1)$$

The momentum equation can be written:

$$-\frac{\partial\phi}{\partial t} + \frac{1}{2}(\mu^2+\nu^2) + \frac{P}{\rho} + gh = 0 \qquad (2)$$

At the surface the average orbital velocity is negligible for small amplitude waves, hence:

$$-\frac{\partial\phi}{\partial t} + \frac{P}{\rho} + gh = 0 \qquad (3)$$

These equations describe the body of the fluid.

There are two boundary conditions:

a) At the bed the fluid particles remain in contact

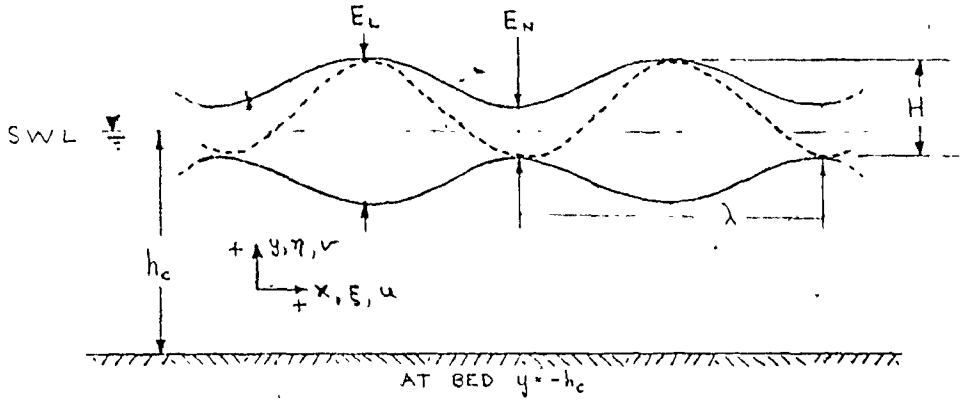

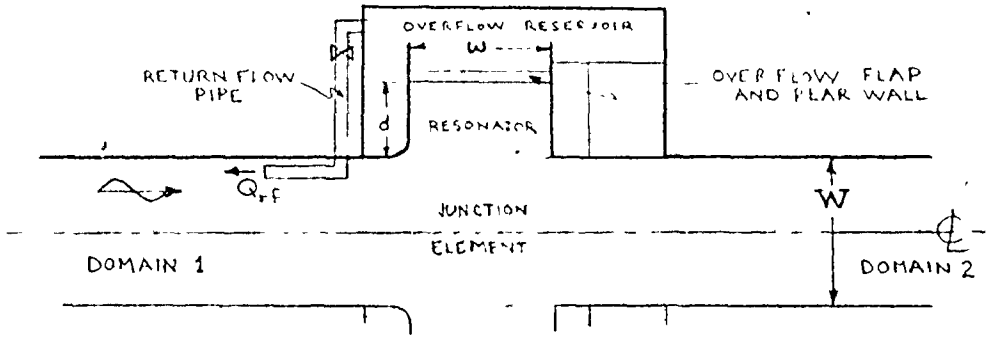

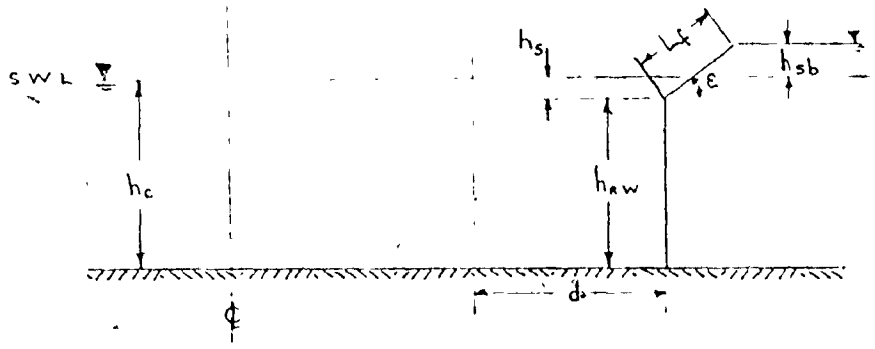

Fig. 2-1 : Notation

with the bed:

$$\left(\frac{\partial \phi}{\partial y}\right)_{y=-h} = 0 \qquad (4)$$

b) At the free surface ($y = 0$), the pressure is zero. Hence from equation (3):

$$\frac{\partial \phi}{\partial t} = g\eta \qquad (5)$$

Since amplitudes are assumed to be small, $h \rightarrow \eta$, hence:

$$\eta = \frac{1}{g} \frac{\partial \phi}{\partial t} \qquad (6)$$

Partial differential equations may be solved by the method of separation of variables, in which a solution is assumed in product form, each term being a function of only one of the independent variables.

The solution is assumed to be:

$$\phi(x,y,t) = X(x) \cdot Y(y) \cdot T(t) \qquad (7)$$

where X is a function of x alone

Y is a function of y alone

and T is a function of t alone.

Substituting equation (7) into equation (1):

$$Y \cdot T \cdot \frac{\partial^2 X}{\partial x^2} + X \cdot T \cdot \frac{\partial^2 Y}{\partial y^2} = 0 \qquad (8)$$

Dividing by $X \cdot Y \cdot T$:

$$\frac{\frac{\partial^2 X}{\partial x^2}}{X} = -\frac{\frac{\partial^2 Y}{\partial y^2}}{Y} \qquad (9)$$

Each term in equation (9) is a function of only one variable and hence each term cannot vary and must be a constant. If this constant is $-k^2$, equation (9) becomes:

$$\frac{\frac{\partial^2 X}{\partial x^2}}{X} = -\frac{\frac{\partial^2 Y}{\partial y^2}}{Y} = -k^2 \qquad (10)$$

Hence two differential equations are formed:

$$\frac{\partial^2 X}{\partial x^2} + k^2 x = 0 \qquad (11)$$

and

$$\frac{\partial^2 Y}{\partial y^2} - k^2 y = 0 \qquad (12)$$

The solutions of which are:

$$X = A \cos kx + B \sin kx$$

$$Y = C\, e^{ky} + D\, e^{-ky}$$

where A, B, C and D are arbitrary constants.

Equation (7) may now be written:

$$\phi(x,y,t) = (A \cos kx + B \sin kx) \cdot (C\, e^{ky} + D\, e^{-ky}) \cdot T(t) \qquad (13)$$

Since solutions which are simple harmonic with respect to time are wanted, it is reasonable to express T (t) as $\cos \sigma t$ or $\sin \sigma t$ where:

$$\sigma = 2\pi / T \quad \text{(angular frequency)}$$

There are four separate elementary combinations of the terms which themselves are solutions to Laplace's equation:

$$\phi_1 = A_1 (C\, e^{ky} + D\, e^{-ky}) \cos kx \cos \sigma t \qquad (14)$$

$$\phi_2 = A_2 (C\, e^{ky} + D\, e^{-ky}) \sin kx \sin \sigma t \qquad (15)$$

$$\phi_3 = A_3 (C\, e^{ky} + D\, e^{-ky}) \sin kx \cos \sigma t \qquad (16)$$

$$\phi_4 = A_4 (C\, e^{ky} + D\, e^{-ky}) \cos kx \sin \sigma t \qquad (17)$$

This facilitates the evaluation of the unknowns and, since

Laplace's equation is linear, the separate solutions may be recombined linearly if necessary.

Using ϕ_1, to solve for the unknowns:

$$\left(\frac{\partial \phi_1}{\partial y}\right)_{y=-h} = A_1 \cos kx \cos \sigma t \{C\, k e^{-kh} - D\, k e^{kh}\} \qquad (18)$$

From equation (4) this must be zero for all x and t thus:

$$C = D\, e^{2kh} \qquad (19)$$

and $$\phi_1 = 2\, A_1\, D\, e^{kh} \cosh k(y+h) \cos kx \cos \sigma t \qquad (20)$$

Then

$$\eta = \frac{1}{g}\left(\frac{\partial \phi_1}{\partial t}\right)_{y=0} = -\frac{2\sigma A_1}{g} D e^{kh} \cosh kh \cos kx \sin \sigma t \qquad (21)$$

The maximum value of η is the amplitude "a", and will occur when $\cos kx \cdot \sin \sigma t = 1$.

Hence $$A_1\, D\, e^{kh} = -\frac{ag}{2\sigma \cosh kh} \qquad (22)$$

and thus $$\eta = a \cos kx \cdot \sin \sigma t \qquad (23)$$

Hence $$\phi_1 = -\frac{ag \cosh k(y+h)}{\sigma \cosh kh} \cos kx \cos \sigma t \qquad (24)$$

In order that ϕ_1, be periodic in x with wavelength λ it is necessary that:

$$k = \frac{2\pi}{\lambda} \quad (\text{wave number})$$

The constants in the other elementary potential function expressions can be evaluated in the same way:

$$\phi_1 = -\frac{ag \cosh k(y+h)}{\sigma \cosh kh} \cos kx \cos \sigma t \qquad (25)$$

$$\phi_2 = +\frac{ag \cosh k(y+h)}{\sigma \cosh kh} \sin kx \sin \sigma t \qquad (26)$$

$$\phi_3 = -\frac{ag \cosh k(y+h)}{\sigma \cosh kh} \sin kx \cos \sigma t \qquad (27)$$

$$\phi_4 = +\frac{ag \cosh k(y+h)}{\sigma \cosh kh} \cos kx \sin \sigma t \qquad (28)$$

These may be combined linearly to form solutions such as:

$$\phi = \phi_2 - \phi_1$$

$$= \frac{ag \cosh k(y+h)}{\sigma \cosh kh} \cos(kx-\sigma t) \qquad (29)$$

or $$\phi = -(\phi_3 + \phi_4)$$

$$\phi = \frac{ag \cosh k(y+h)}{\sigma \cosh kh} \sin(kx-\sigma t) \qquad (30)$$

From these expressions the equations for particle displacement and velocities can be derived:

$$\mu = -\frac{\partial \phi}{\partial x} = \frac{agk}{\sigma} \frac{\cosh k(y+h)}{\cosh kh} \sin(kx-\sigma t) \qquad (31)$$

$$\upsilon = -\frac{\partial \phi}{\partial y} = -\frac{agk}{\sigma} \frac{\sinh k(y+h)}{\cosh kh} \cos(kx-\sigma t) \qquad (32)$$

Integration of the velocity term with respect to time provides the particle displacements:

$$\xi = \int \mu \, dt = \frac{agk}{\sigma^2} \frac{\cosh k(y+h)}{\cosh kh} \cos(kx-\sigma t) \qquad (33)$$

$$\eta = \int u \, dt = \frac{agk}{\sigma^2} \frac{\sinh k(y+h)}{\cosh kh} \sin(kx-\sigma t) \qquad (34)$$

2.3 Potential Energy

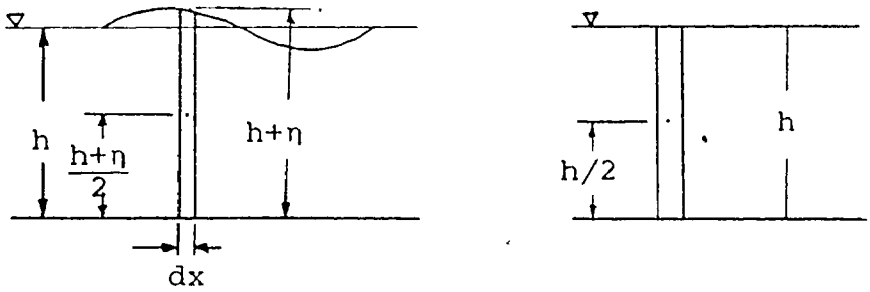

The potential energy in a progressive wave is that due to the wave deformation from the still water level, minus the potential energy of the water in the absence of any wave. The average potential energy per unit surface area is :

$$\overline{E}_p = \frac{\gamma}{2\lambda T} \int_0^T \int_0^\lambda (h+\eta)^2 dx dt \qquad (35)$$

Substituting $\eta = \frac{H}{2} \sin(kx-\sigma t)$ into (35):

$$\overline{E}_p = \frac{\gamma}{2\lambda T} \int_0^T \int_0^\lambda (h+ \frac{H}{2} \sin(kx-\sigma t))^2 \, dx dt \qquad (36)$$

Simplifying and substituting identity (A), page 27, gives:

$$\overline{E}_p = \frac{\gamma}{2\lambda T} \int_0^T \{H^2 x - \frac{Hh}{k} \cos(kx-\sigma t) + \frac{H^2}{8}(x - \frac{1}{2k} \sin 2(kx-\sigma t))\}_0^\lambda \, dt \qquad (37)$$

Expanding $\cos(kx-\sigma t)$ and $\sin(kx-\sigma t)$ with identities (B) and (C) and simplifying :

$$\bar{E}_p = \frac{\gamma}{2\lambda T} \int_0^T h^2\lambda + \frac{H^2\lambda}{8}\, dt \qquad (38)$$

which reduces to :

$$\bar{E}_p = \frac{\gamma h^2}{2} + \frac{\gamma H^2}{16} \qquad (39)$$

The potential energy in the absence of a wave is :

$$\bar{E}_p = \frac{\gamma}{2\lambda T} \int_0^T \int_0^\lambda h^2\, dxdt \qquad (40)$$

$$= \frac{\gamma h^2}{2}$$

Thus the average potential energy per unit surface area due to the presence of a wave is :

$$\bar{E}_p = \frac{\gamma h^2}{2} + \frac{H^2\gamma}{16} - \frac{\gamma h^2}{2} \qquad (41)$$

$$= \frac{\gamma H^2}{16}$$

2.4 Kinetic Energy

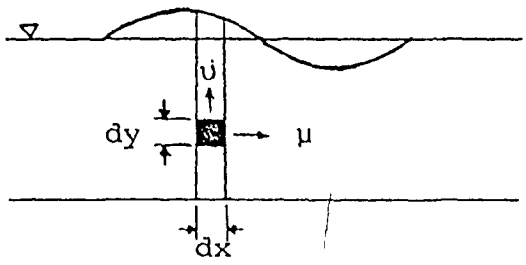

The average kinetic energy per unit of surface area is given by :

$$\bar{E}_k = \int_0^T \int_0^\lambda \int_{-h}^0 \frac{\rho}{2\lambda T} (\mu^2+\upsilon^2)\ dydxdt \qquad (42)$$

Substituting for μ and υ and simplifying :

$$\bar{E}_k = \frac{g\gamma a^2k^2}{2\lambda T\sigma^2\cosh^2kh}\int_0^T\int_0^\lambda\int_{-h}^0 \{\cosh^2k(y+h)\sin^2(kx-\sigma t)+ \sinh^2k(y+h)\cos^2(kx-\sigma t)\}\ dydxdt \qquad (43)$$

Substituting identities (D),(E),(F) and (G) into equation (43) and simplifying :

$$\bar{E}_k=\frac{g\gamma a^2k^2}{4\lambda T\sigma^2\cosh^2kh}\int_0^T\int_0^\lambda\int_{-h}^0 \{\cosh 2k(y+h)-\cos 2(kx-\sigma t)\}dydxdt \qquad (44)$$

After integrating :

$$\bar{E}_k = \frac{\gamma H^2 \cdot gk \cdot \tanh\ kh}{16\sigma^2} \qquad (45)$$

Since $\sigma^2 = gk\cdot\tanh(kh)$, equation (45) reduces to :

$$\bar{E}_k = \frac{\gamma H^2}{16} \qquad (46)$$

2.5 Continuity Equation

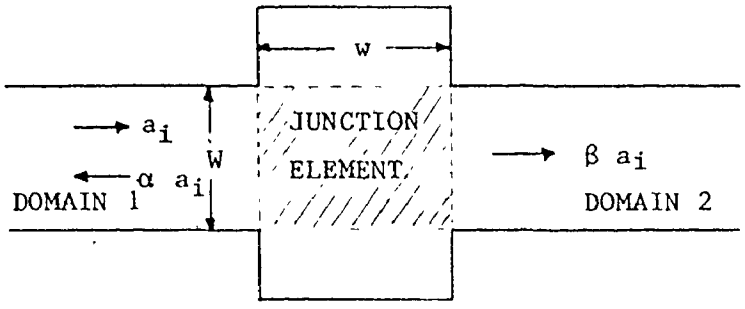

A continuity equation for the junction element may be

formulated as follows :

$$I_e - O_e - 2Q_{rf} = A_e \left(\frac{\partial \bar{\eta}}{\partial t} \right) \qquad (47)$$

where I_e = flow into junction element

O_e = flow out of junction element

and A_e = surface area of junction element (W·w)

The partial derivative of the average vertical surface displacement with respect to time cannot be evaluated at this time, preventing further development along these lines.

2.6 Return Flow

The return flow mechanism is a dynamic system and thus; for simplification, some averaging must be incorporated in the equations describing it's behaviour.

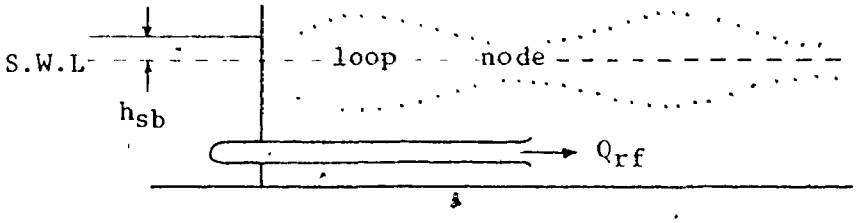

It is necessary to use average values for both stilling basin height and discharge, due to the fluctuations in water surface elevation above the discharge in the main channel. This head fluctuation across the return flow pipe greatly affects discharge uniformity due to the relative magnitude of the stilling basin head developed. The orbital motions at the discharge also affects the uniformity, if the discharge is not deeper than twice the incident

wavelength. The effect of both inertial and frictional drag on the fluid in the pipe tends to help dampen out the fluctuations somewhat. The fluctuation of the stilling basin depth can be minimized by providing a large holding basin or reservoir from which the return flow discharge may be drawn. Thus it seems reasonable to develop an expression in terms of the average head and discharge.

2.7 Power

Wave power is the time rate at which work is done by a wave. It is well known that wave energy propagates at the group velocity C_G where :

$$C_G = \frac{C}{2} \left\{ 1 + \frac{2kh}{\sinh 2kh} \right\} \qquad (48)$$

and C is the phase velocity of the individual waves. The energy propagated is the total wave energy, which is the sum of both kinetic and potential wave energies. Thus total average wave power over one wave period per foot of width may be written :

$$\overline{P}_{to} = \overline{E}_{to} \cdot C_G = \frac{\lambda \gamma H^2}{8} \cdot C_G \qquad (49)$$

Power in flowing water, as in pipes, is calculated by multiplying the number of pounds of fluid flowing per second, by the energy lost or gained across the control section. This results in an equation of the form :

$$P = \gamma Q h \tag{50}$$

From equations (49) and (50) we now have expressions for all the energies involved in the junction element except for losses due to eddy formation and turbulence. Summarizing we have :

$$\overline{P}_{to} = \frac{W\lambda\gamma H^2}{8} \cdot C_G \tag{51}$$

which represents the total wave power in a channel of width " W " feet. This applies to all waves including incident, reflected and transmitted, and is differentiated by subscripting the wave height term; and :

$$\overline{P}_{rf} = 2\gamma \overline{Q}_{rf} \overline{h}_{sb} \tag{52}$$

which represents the total average return flow power from both resonators.

By performing a power balance on the junction element, it is possible to develop an expression for the average return flow that might be expected from the operation of a return flow resonator. Balancing the power terms we have :

$$\overline{P}_i = \overline{P}_r + \overline{P}_t + \overline{P}_{rf} + \text{power losses} \tag{53}$$

Substituting for each term gives :

$$\frac{W\gamma H_i^2}{8} \cdot C_G = \frac{W\gamma H_r^2}{8} \cdot C_G + \frac{W\gamma H_t^2}{8} \cdot C_G + 2\gamma \overline{Q}_{rf} \overline{h}_{sb} \tag{54}$$

Substituting :

$$H_r^2 = \alpha^2 H_i^2 \quad \text{and} \quad H_t^2 = \beta^2 H_i^2 \tag{55}$$

and reducing gives :

$$\overline{Q}_{rf} = \{ 1 - (\alpha^2+\beta^2) \} \frac{WH_i^2}{16h_{sb}} \cdot C_G \qquad (56)$$

For perfect reflection or transmission, the return flow will be zero. The return flow would only be dependant on W for $W \leq \lambda$. For W larger than λ , energy will be transmitted into the harbour and not greatly affected by the resonators. This equation of course does not relate Q_{rf} to w or d directly, but, α and β values are highly dependant on both " w " and " d ".

"IDENTITIES" USED

(A) $\sin^2 (kx - \sigma t) = 1/2(1 - \cos 2(kx - \sigma t))$

(B) $\cos(kx - \sigma t) = \cos kx \cos \sigma t + \sin kx \sin \sigma t$

(C) $\sin 2(kx - \sigma t) = \sin 2kx \cos 2\sigma t - \cos 2kx \sin 2\sigma t$

(D) $\cosh^2 k(y+h) = 1/2(1 + \cosh 2k(y+h))$

(E) $\sinh^2 k(y+h) = -1/2(1 - \cosh 2k(y+h))$

(F) $\cos^2(kx - \sigma t) - \sin^2(kx - \sigma t) = \cos 2(kx - \sigma t)$

(G) $\cos^2(kx - \sigma t) + \sin^2(kx - \sigma t) = 1$

(H) $\sinh 2kh = 2 \sinh kh \cos kh$

(I) $\sigma^2 = gk \tanh kh$

APPARATUS

3.1 Wave Flume

In designing the wave flume it was necessary to allow for the installation of all essential wave devices. For each of the two absorbers, two filter banks and resonator test section, distances at least equal to the maximum test wavelength were allowed. For each of the two measuring domains, distances equal to three maximum wavelengths were allowed. The experimental apparatus used in the study comprised a wave flume measuring 44 feet long, 2 feet wide by 1 foot deep with a central resonator basin 4 feet long and 6 feet wide as shown in Figure 3-1. Clear plexiglass walls were provided adjacent to the resonator basins. A false concrete bed approximately 3/8 inches thick was placed in the flume to provide a uniform depth throughout the length and width of the tank.

3.2 Absorbers

At the extreme ends of the tank, wave absorbers 4 feet in length, as described by Lean[19] fabricated from 1/4 inch steel plate; with 1/2 inch diameter holes drilled evenly on a two inch square grid, were rigidly fixed to the channel end walls. The downstream absorber was also fitted

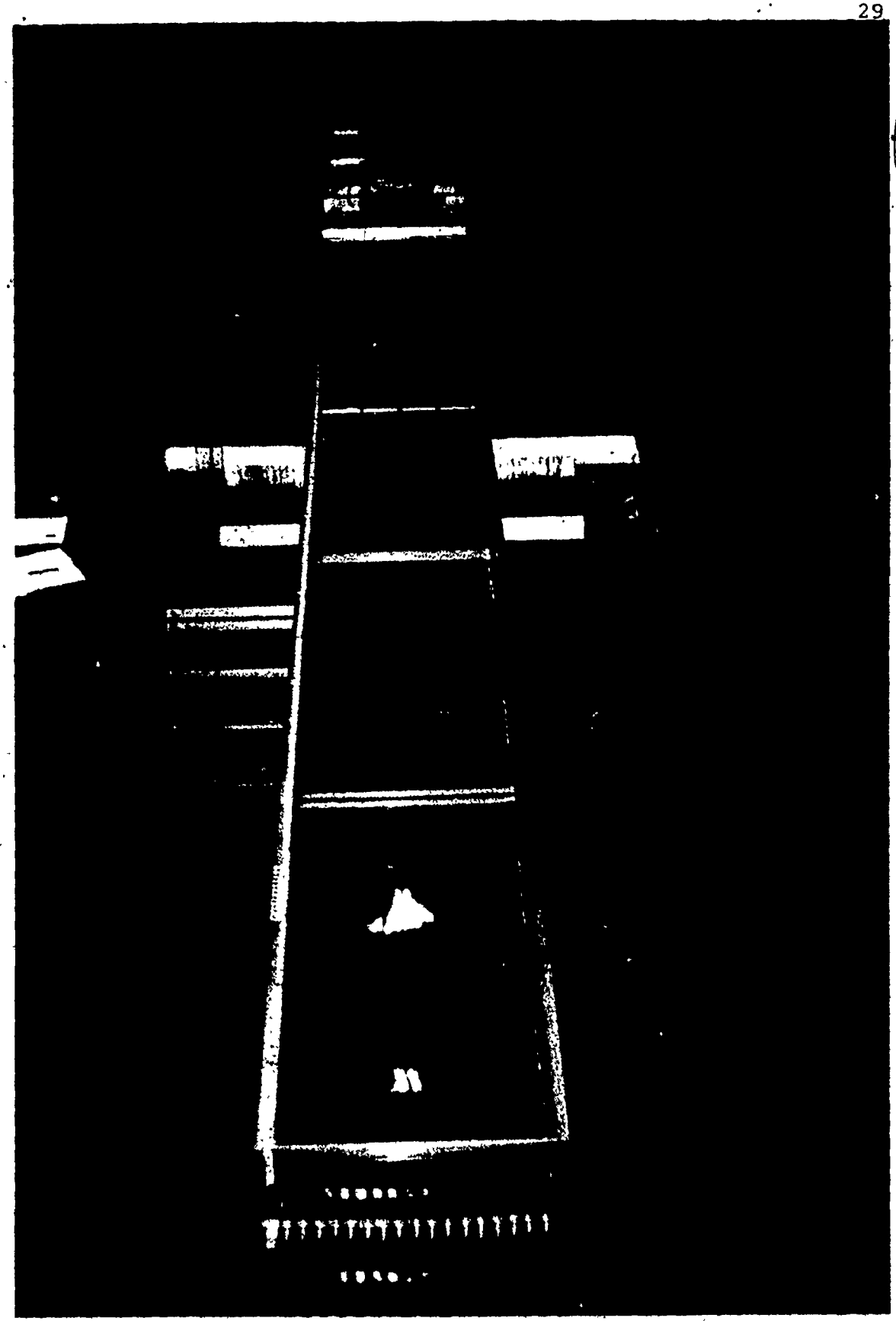

Fig. 3-1 : Wave Flume

with sheets of 1/2 inch thick fibreglass matting as shown in Figure 3-2 to further reduce wave reflection as described by Garrett[6]. This will produce a better decoupling of the system. Permeable absorbers such as these are particularly suited to low waves which are harder to absorb than steep waves. With these absorbers, steep waves tend to break upon entry; energy losses due to breaking are much greater than the energy losses due to friction and eddy formation. Lean states[19] that energy dissipation is a function of wave amplitude, i.e. losses are proportional to the depth at breaking and/or the height of the breaker.

3.3 Wave Generator

At the extreme upstream end immediately adjacent to the wave absorber, a paddle-type wave generator was installed consisting of a plate linked by a drive arm to an electrically driven eccentric as shown in Figure 3-3. Both eccentricity and linkage length were variable so that paddle stroke and position could be adjusted. The waves generated were approximately one inch in height. The linkage connections remained constant throughout the test period, with the result that wave amplitudes varied and were frequency dependent. However the maximum wave steepness of 0.055 was such that linear theory was still appropriate. The drive mechanism included a low horsepower A.C. motor with both a gear reduction and pulley reduction system to allow

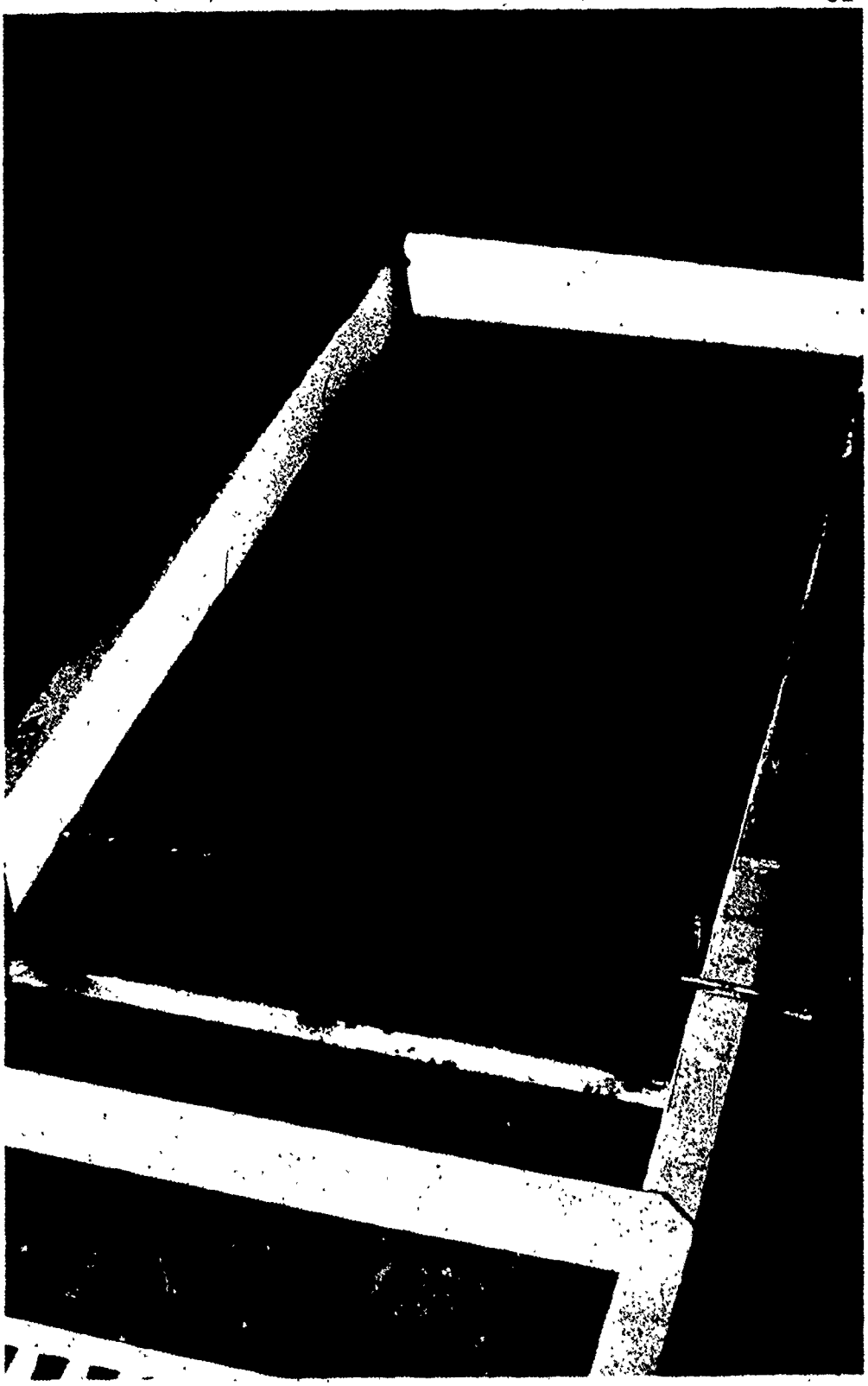

Fig. 3-2 : Absorber with fibreglass matting

Fig. 3-3 : Wave Generator

motor speeds to considerably exceed the wave generator speeds. This ensured regularity in the periods and sinusoidal profile of the waves generated. The mechanism was controlled remotely by a rheostat at the resonators and successfully produced a monoperiodic wave train.

3.4 Low Pass Filters

Immediately adjacent to the wave generator and wave absorbers, a system of low pass filters was installed. These filters improved the uniformity of the monoperiodic wave train by eliminating the harmonics of higher frequency that were generated. The filters were constructed of aluminium tubing to form a framework, over which continuous fibreglass screening was stretched so as to form a series of vertical panels, aligned in the orbital planes, spaced at 1/2 inch intervals across the width and extending to full depth of the tank as shown in Figure 3-4. Each of these filters was approximately 2 feet long by 2 feet wide to enable rigid installation in the flume. A each end, two of these filters were used in series to ensure that the length exceeded the maximum wavelength to be tested, as described by James[10]. The performance of such filters is amplitude independent but frequency dependent in that transmissivity increases with increasing wave period.

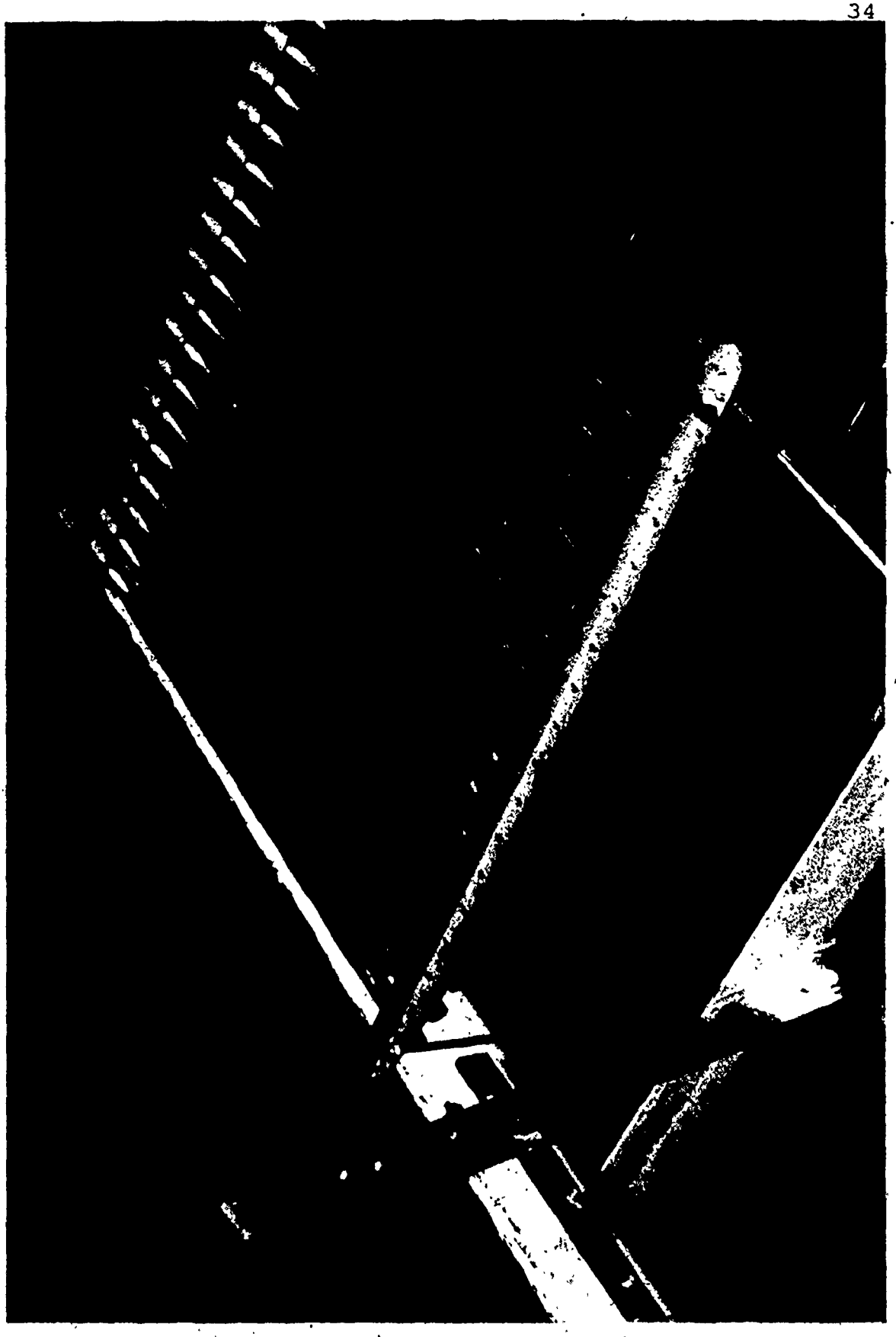

Fig. 3-4 : Low Pass Filter

3.5 Wave Guides

In the upstream domain between the resonators and the filters, a wave guide was installed to prevent transverse oscillations in the tank. Such transverse resonance occurs at frequencies whose wavelengths are near or at multiples of the tank width. The wave guides consisted of aluminium screening stretched parallel to the tank walls positioned at the nodal points for the fundamental transverse resonant frequency as shown in Figure 3-5.

3.6 Instrumentation

On the central 25 feet of the tank a system of horizontal elevated aluminium rails was constructed to accommodate the instrumentation trolly. These rails were brought to uniform height above the water surface by adjustment of the threaded supports and use of an engineer's transit. The instrumentation trolly was fabricated from extruded aluminium sections and rode on three free turning brass wheels as illustrated in Figure 3-6. The trolly carried a micrometer with 2 inch travel, set in a steel support frame. A long needle probe of appropriate length was attached to the micrometer head for accurate measurement of wave envelopes. The probe was insulated from the carriage frame and connected directly to a cathode ray oscilloscope as shown in Figure 3-7. Determination of probe entry and

Fig. 3-5 : Wave Guides

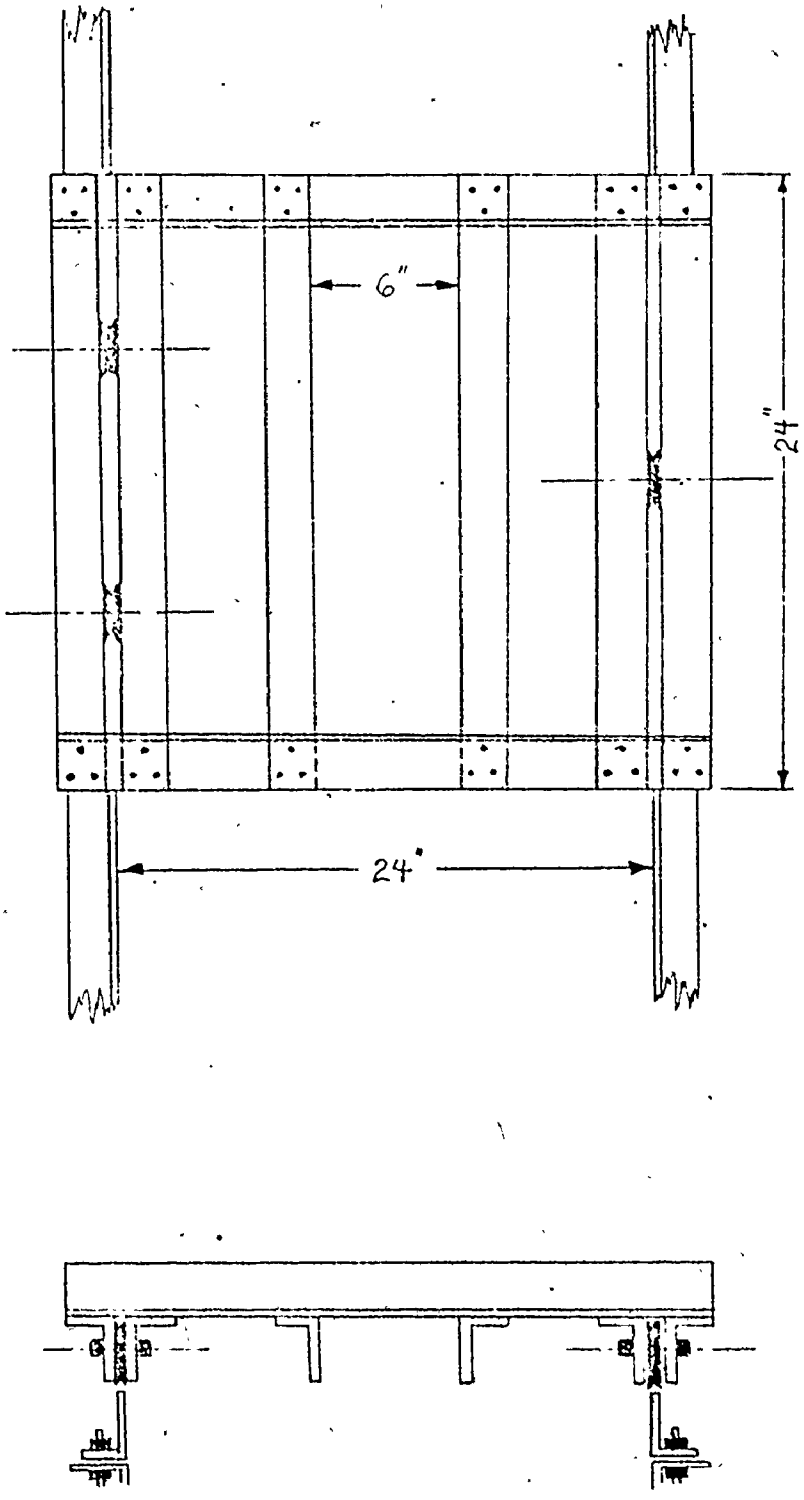

Fig. 3-6 : Instrumentation Trolly

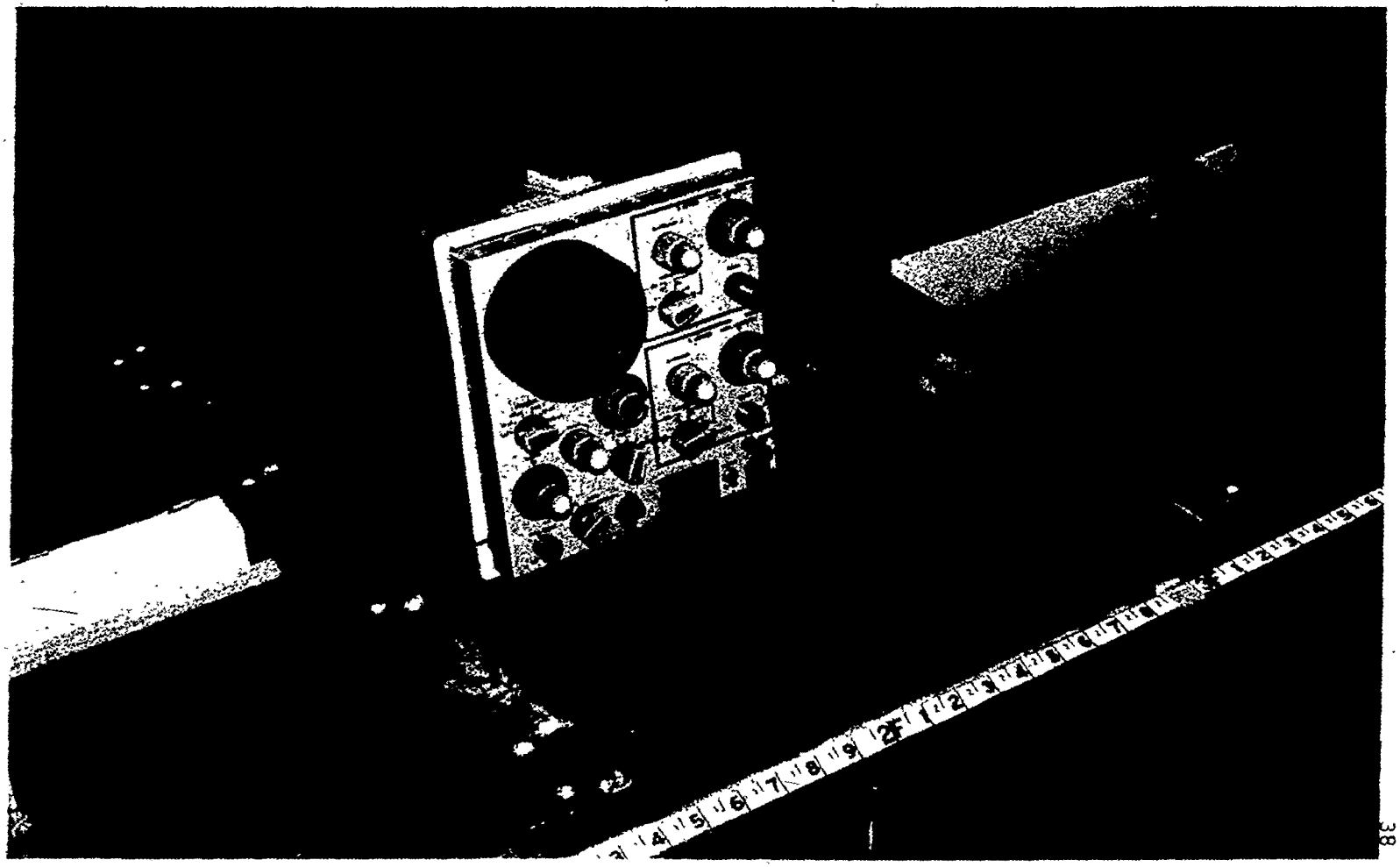

Fig. 3-7 : Wave Measurement Apparatus

exit points was thus more precise than visual observations would be.

3.7 Resonator Chambers

At the channel mid-point, a resonator and junction element with a total width of 6 feet, was provided. This section covered the central 4 feet of the tank. Within this area on each side of the tank, two false walls were constructed to provide a lateral base for the resonators. The downstream wall was a "⊔" section installed so that one leg of the section was in line with the main channel wall while the open end faced the wall of the expansion chamber as shown in Figure 3-8. The upstream wall was an "L" section with a circular re-entrant curve instead of a sharp 90 degree corner. This curve effectively reduced turbulent eddies that resulted from the high velocities produced when the incident wave fronts expand at this point. These two sections formed the side walls of the resonators. The rear walls were constructed from 1/16 inch steel plate. The rear wall had to be hinged to provide an adjustable overflow flap. The vertical section of the rear wall was 6-1/2 inches high and the movable flap section was 2-1/2 inches wide so that when the flap section was vertical the total height of the rear wall was approximately 9 inches as shown in Figure 3-9. The water depth during the tests was held constant at 7-1/2 inches. The hinge comprised

Fig. 3-8 : Resonator Chamber

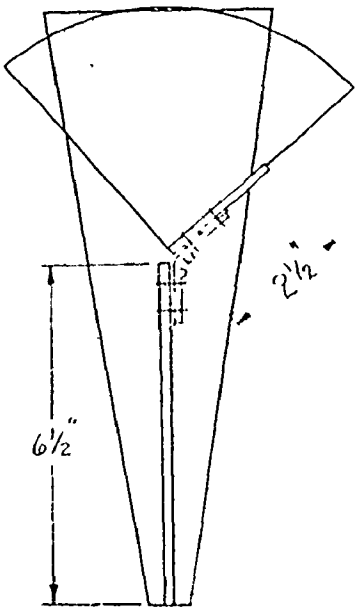

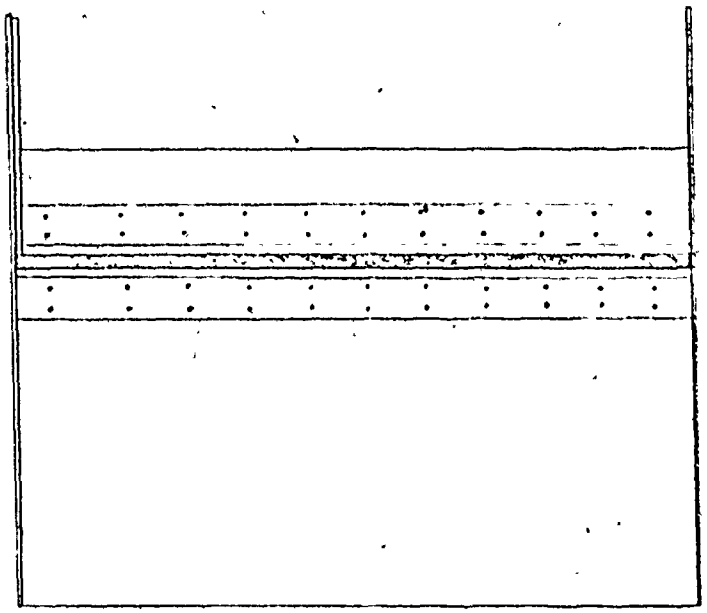

Fig. 3-9 : Hinged Rear Wall Assembly

an overlapping rubber strip bolted to each section of the rear wall as shown in Figure 3-10. This provided a water tight hinge which was considered essential. This rear wall was simply clamped in place for testing. A number of "⊔" shaped walls were used to systematically reduce the resonator width simply by adding them one at a time to the existing wall already secured in the tank as shown in Figure 3-8. Each time an additional "⊔" wall was added the rear wall was accordingly cut down in length. These false walls in the expansion section provided a storage area for the overflow from the resonators. Large quantities of fibreglass screening was packed in the stilling chamber to prevent oscillations. A plexiglass chamber approximately 14 inches high was secured to the rear wall of the overflow basin. This 4 inch by 4 inch square chamber had two 1/16 inch diameter holes drilled in its base below normal still water depth. This allowed the water level inside the tower to rise and fall slowly according to the water level in the overflow basin. A 2 inch travel micrometer with a needle probe attachment was used to monitor fluctuations in the overflow basin water depth as illustrated in Figure 3-11.

3.8 Return Flow Arrangement

A 3/4 inch diameter pipe was attached to the rear corner of each upstream wall and passed externally back

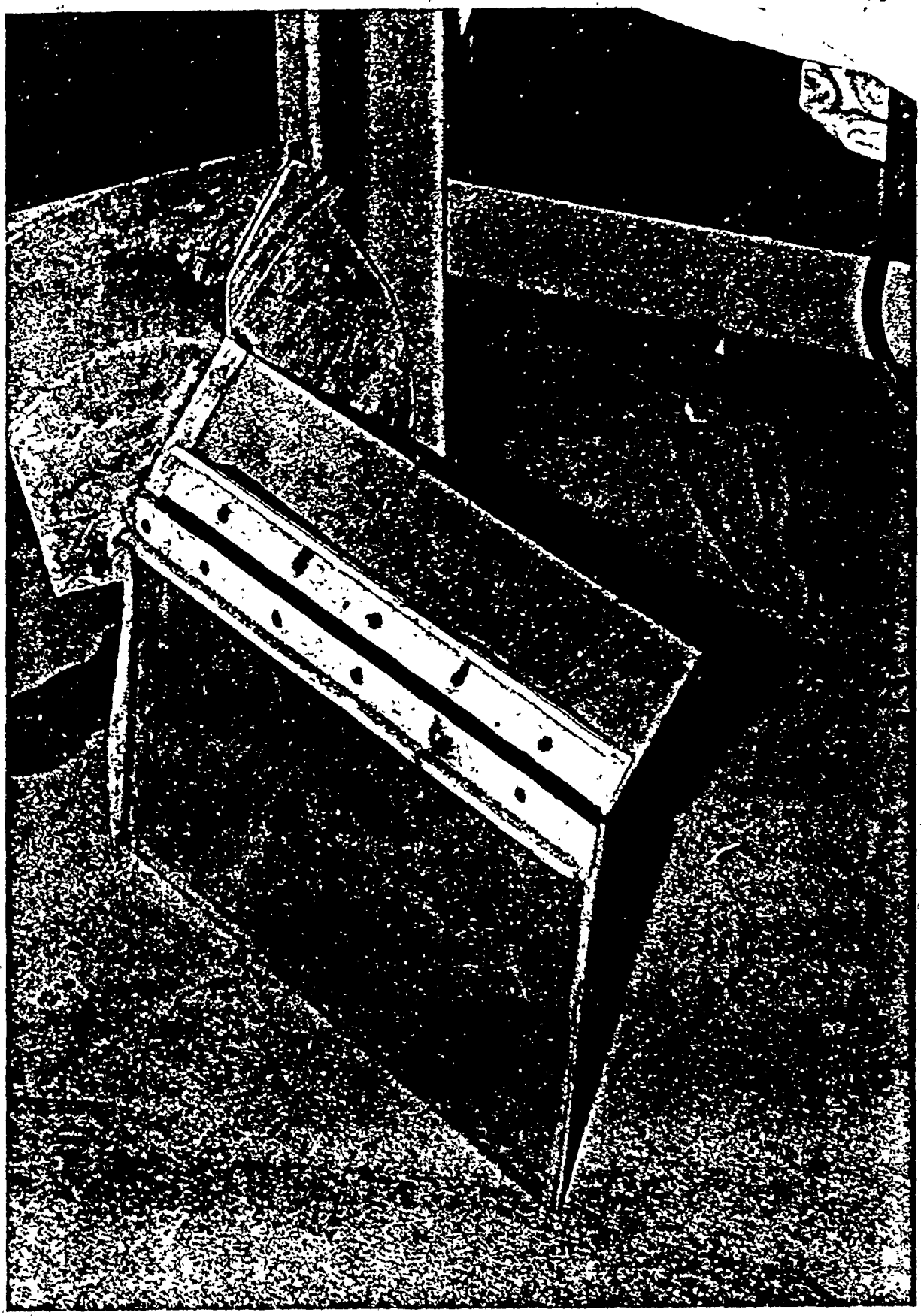

Fig. 3-10 : Rear Wall Construction

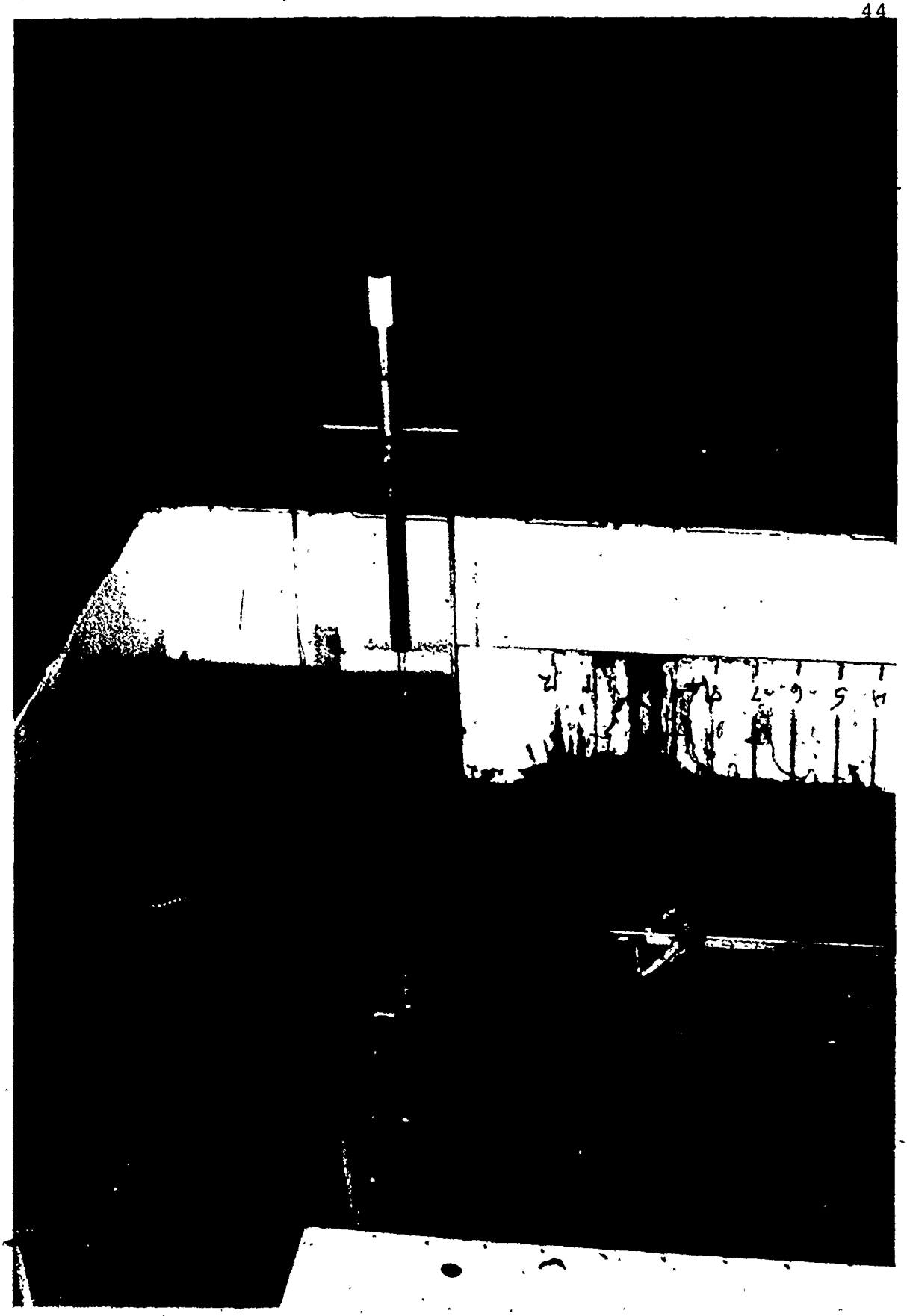

Fig. 3-11 : Overflow Monitoring Tower

into the main channel entering in an upstream direction. A control valve was placed in each of these return flow pipes to interrupt the flow returning to the main channel. A vertical overflow was provided as shown in Figure 3-12, free to rotate in a vertical circle. At the start of each test the overflow invert was set to the same level as the main channel water level. Once the test had started, resonator overflow discharge from this pipe; with the return flow valve shut, was measured using a stopwatch and a 500 millilitre graduated cylinder. The overflow was caught in a large drum and pumped back into the main tank behind the wave generator by means of a small submersible bilge pump. This maintained a constant water depth throughout the test period.

Fig. 3-12 : Return Flow Arrangement

EXPERIMENTAL PROCEDURE

4.1 Wavelength Calibration

Before experiments on the resonator arrangement could begin, it was necessary to evaluate the characteristics of the tank itself. The flume was first examined to determine the best operating depth. The criteria for "best depth" was the correlation between first order theoretical wavelengths and generated measured wavelengths. Generated wavelengths were measured by observing crest to crest distances against a tape secured to the elevated rails. A number of tests were performed at various depths and wavelengths given by:

$$\lambda = \frac{gT^2}{2\pi} \tanh \frac{2\pi h}{\lambda}$$

were plotted against observed wavelength. The best depth is given by the best linear fit to a line drawn at 45 degrees, making due allowance for the limitations of the measuring equipment and testing facilities. Inspection of Figure 4-1 indicates that a depth of 7 1/2 inches provides a good relationship within the limits of the measuring instruments.

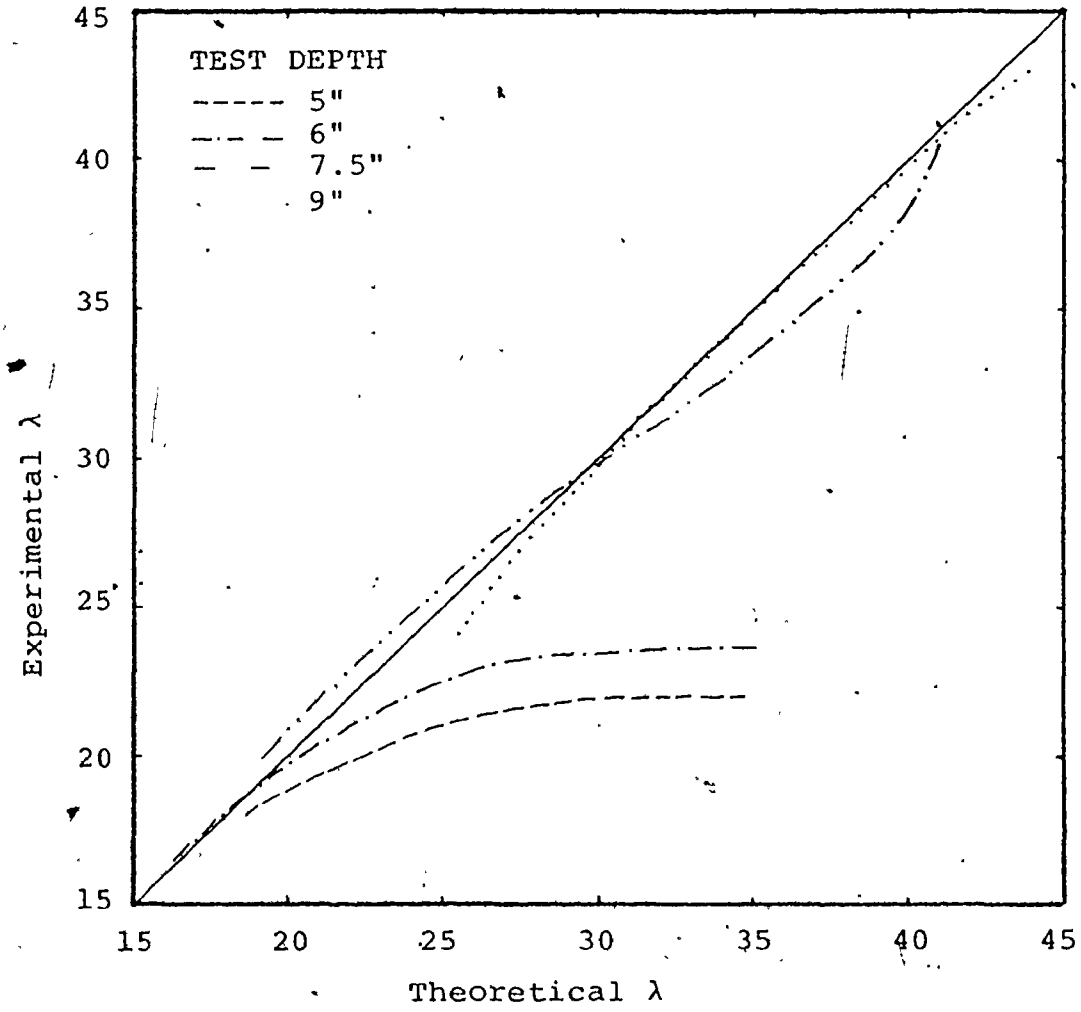

Fig. 4-1 : Theoretical and Experimental Wavelength Relations

4.2 Reflectivity and Transmissivity Calibration

The second consideration was an evaluation of the reflectivity and transmissivity transfer functions, with the resonators isolated from the main channel. That is, the behaviour of the flume decoupling system alone was evaluated as a function of incident wave period. Envelope loop and node heights were measured in both the upstream (Domain 1) and downstream (Domain 2) regions and resulting values of transmissivity and reflectivity were plotted against wave period. Figure 4-2 shows the results of the second test series and indicates that both transfer functions are approximately linear over the range of periods of interest in this study. Thus the frequency band indicated would be satisfactory for testing the resonator configuration.

4.3 Resonator Geometry Limits

These periods also dictated the range of resonator dimensions to be tested as shown by James[12], since it was felt that maximum overflow conditions would be at or near resonant geometries. For wave periods ranging from 0.60 seconds to approximately 1.5 seconds, it was evident that resonator test width "w" ranging from 21 inches to 12 inches and resonator test depths "d" ranging from 9 inches to 4 inches would cover the required range of resonant

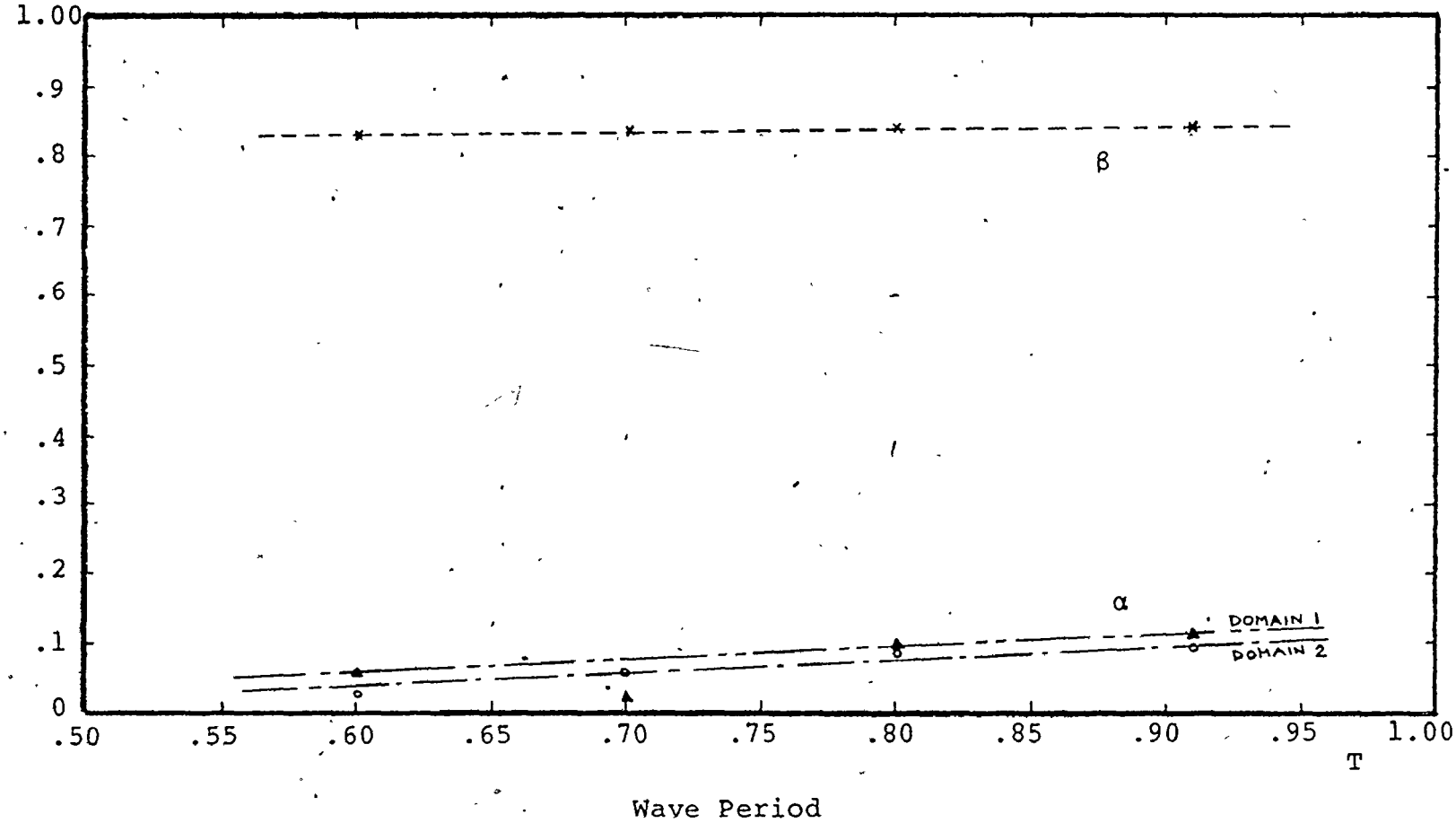

Fig. 4-2 : Transfer Functions for Flume System

geometries. In fact such resonator shapes would vary between the expansion chamber resonant mode and the branch canal resonant mode[13] and should cover the best mode of operation for maximizing return flow energies and minimizing transmitted wave energies.

4.4 Test Procedure for Variation of Geometry

In order to expedite the large number of tests it was decided that the geometry would be held constant while the wave periods varied over the full range. The resonator depth "d" was varied in one inch steps from 9 inches to 4 inches. Once all resonator depths "d" had been tested; each for the full frequency range, the tank was drained and resonator width "w" was then decreased by welding into place the next "⊔" shaped wall section. The rear wall was then simply cut to the new width and refitted for the next test series for depths and periods. For each geometry and test period the following were measured:

a) upstream maximum and minimum envelope heights
b) downstream wave height
c) stilling basin depth increase
d) overflow discharge.

4.5 Loop and Node Technique for Domain 1

The upstream envelope node and loop amplitudes were measured by placing the micrometer probe at a trial depth

and successively lowering or raising until the wave envelope was delineated by the signal on the C.R.O.. The loop or node positions were found by bisecting the position of two equal envelope heights as shown in Figure 4-3. The probe was then positioned at the mid-point and probe depth set, so that at least ten consecutive pulses were observed. This ensured that high or low waves due to parasitic or seiche oscillations were not measured. The loop and node method is based on the assumption that the incident wave form is sinusoidal. Real laboratory waves are significantly trochoidal. This difference introduces some error in the analysis of the partial clapotis envelope and according to James[15], gives a larger value than is indicated by first order theory. The alternate measurement technique called the "Three Point Method"; in which envelope heights are measured at three points one-eighth wavelength apart, may give an unreliable reflectivity at high reflectivities. The downstream wave height was measured at two stations separated by 1/4 of the generated wavelength[16]. The transmitted wave amplitude as given by the average of these two readings would not be in error due to the reflections from the downstream absorber and filter.

4.6 Return Flow Measurement

The discharge was naturally related to the stilling basin depth increase and thus a steady state condition had

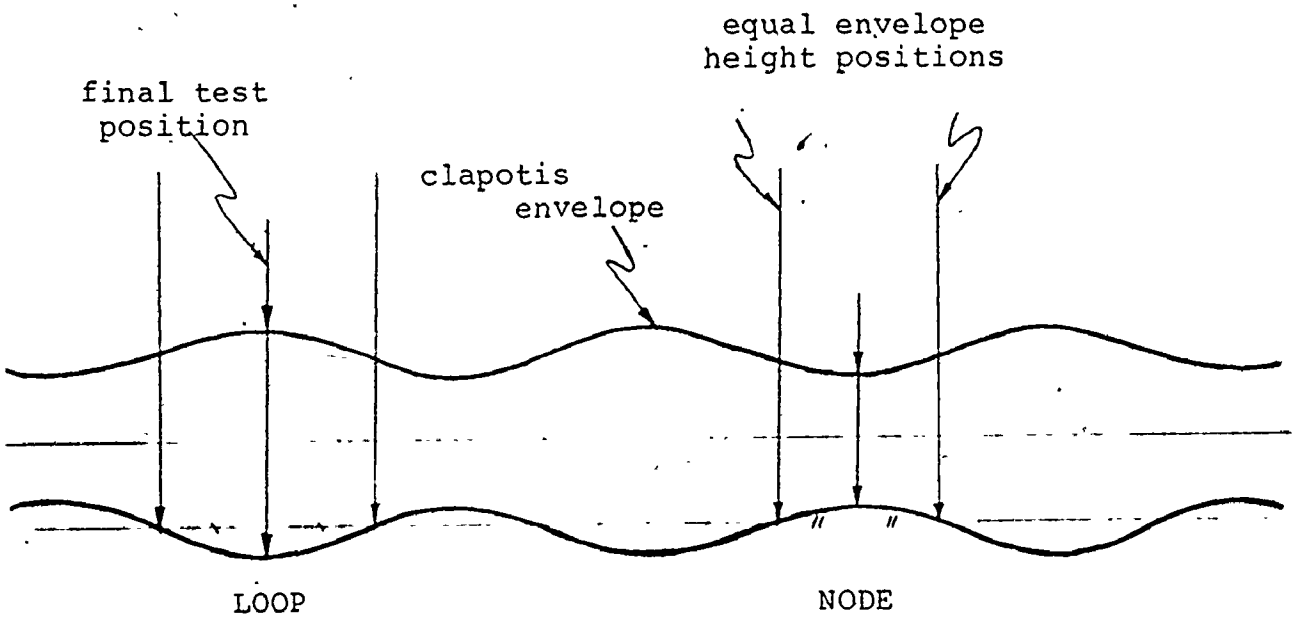

Fig. 4-3 : Bisection Method for Loop and Node Measurement

to be achieved before measurements could be taken. This measurement was the last to be taken in all test series. The position of the overflow flap was critical in the discharges obtained. It was observed that if the overflow flap was low, excessive back wash over the flap would take place. If the flap was too steep the stilling basin water level would be lower than the crest of the overflow flap. The most effective position was set manually by observing the system in operation. The "best" position was such that a small quantity of backwash was allowed. This produced maximum discharges and stilling basin depths. In other words, a trial and error procedure was adopted to produce maximum stilling basin depths. The overflow discharge was then measured by observing the time taken to fill a 500 millilitre measuring cylinder. Each discharge was measured at least three times to ensure accuracy of measurement and uniformity of flow.

4.7 Control of Experiments

The incident wave period was measured both prior to and immediately following the test procedure. The wave period was measured over a two minute interval to achieve the required accuracy. This was particularly necessary when obtaining the peak values of "θ", the ratio of the return flow power to the incident wave power. All data measured were reduced and plotted immediately so that the resulting

curves were well defined at all points. Any anomalies encountered were immediately re-examined and either corrected or noted.

EXPERIMENTAL RESULTS

5.1 Return Flow

The simple relationship used to express the effectiveness of the return flow resonator is termed the "power extraction coefficient", θ . It is a measure of the ratio of return flow power to available incident wave power. The incident wave power is given by:

$$P_i = \frac{W\lambda\gamma H_i^2}{8} \cdot C_G \qquad (1)$$

Return flow power is given by:

$$P_{rf} = \gamma Q_{rf} h_{sb} \qquad (2)$$

This ratio is plotted against the tuning parameter d/λ for different values of d/w, producing families of response curves for each w/W ratio tested in Figures 5-1 to 5-4.

5.2 Transmissivity

Transmissivity is the ratio of the amplitude of the wave transmitted into the harbour past the resonators to the amplitude of the incident wave usually denoted "β", and also known as the coefficient of transmission:

$$\beta = \frac{a_t}{a_i} \text{ or } \frac{H_t}{H_i} \qquad (3)$$

β is also plotted against d/λ for different values of d/w again producing families of curves for each w/W ratio

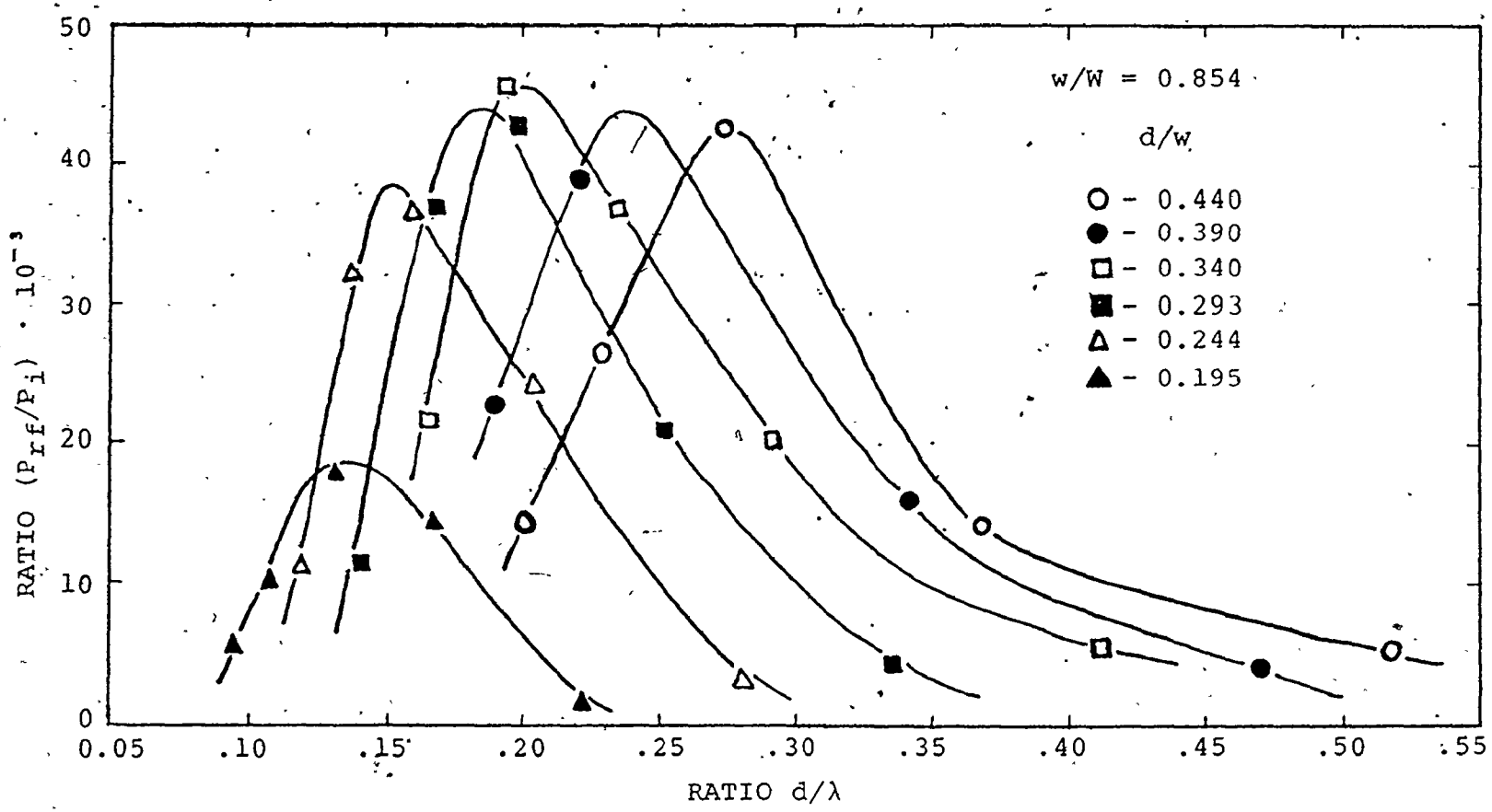

Fig. 5-1 : Power Extraction Coefficient

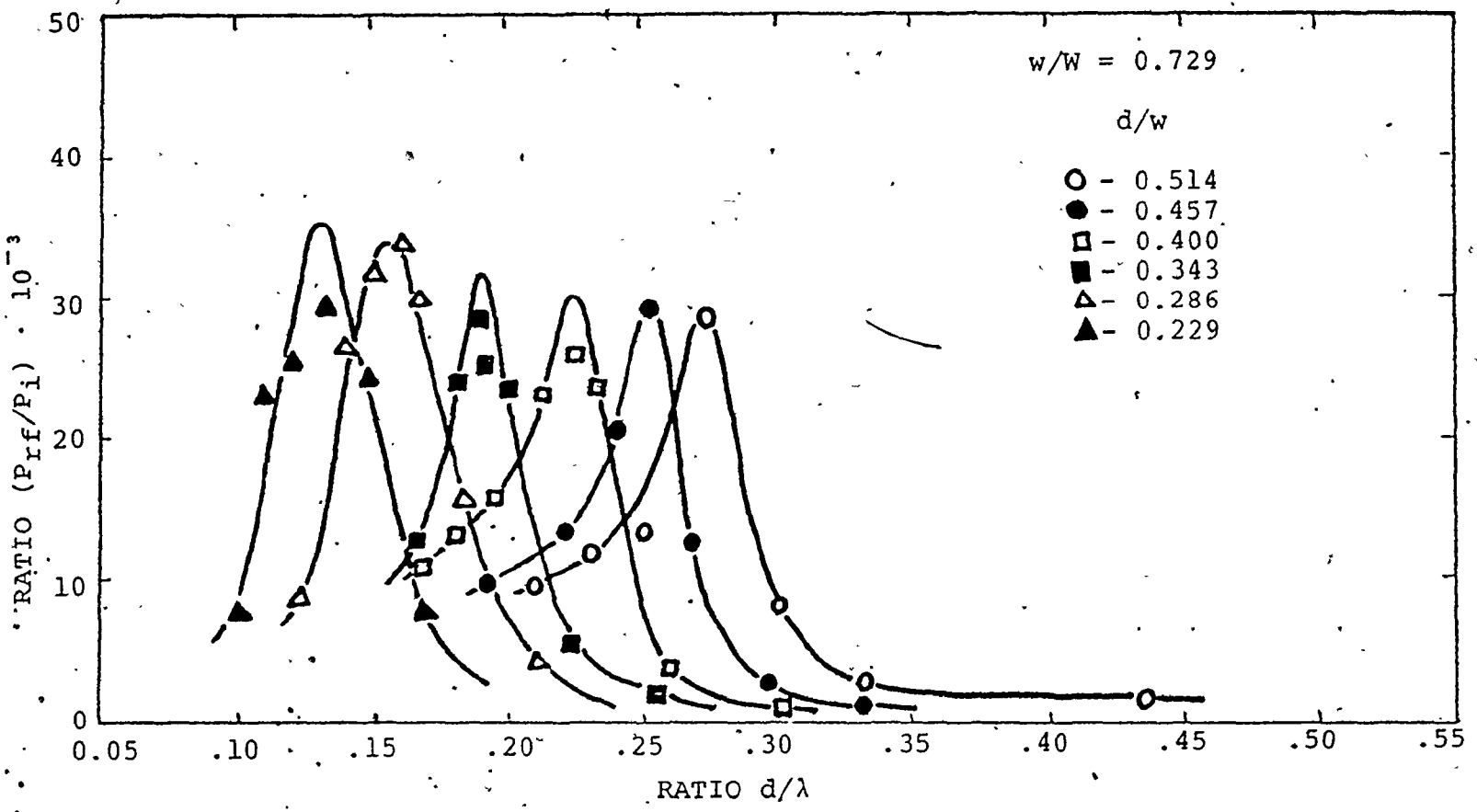

Fig. 5-2 : Power Extraction Coefficient

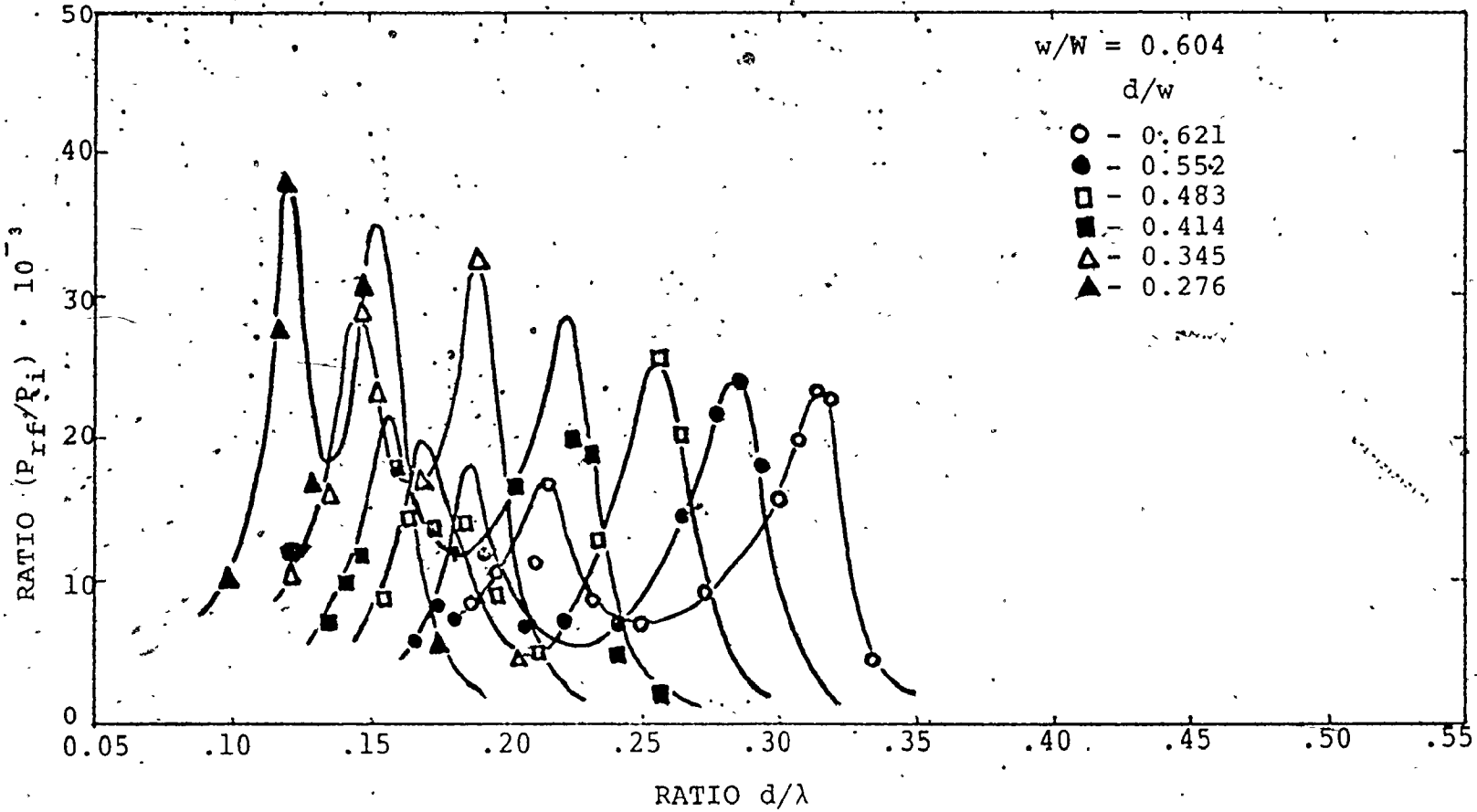

Fig. 5-3 : Power Extraction Coefficient

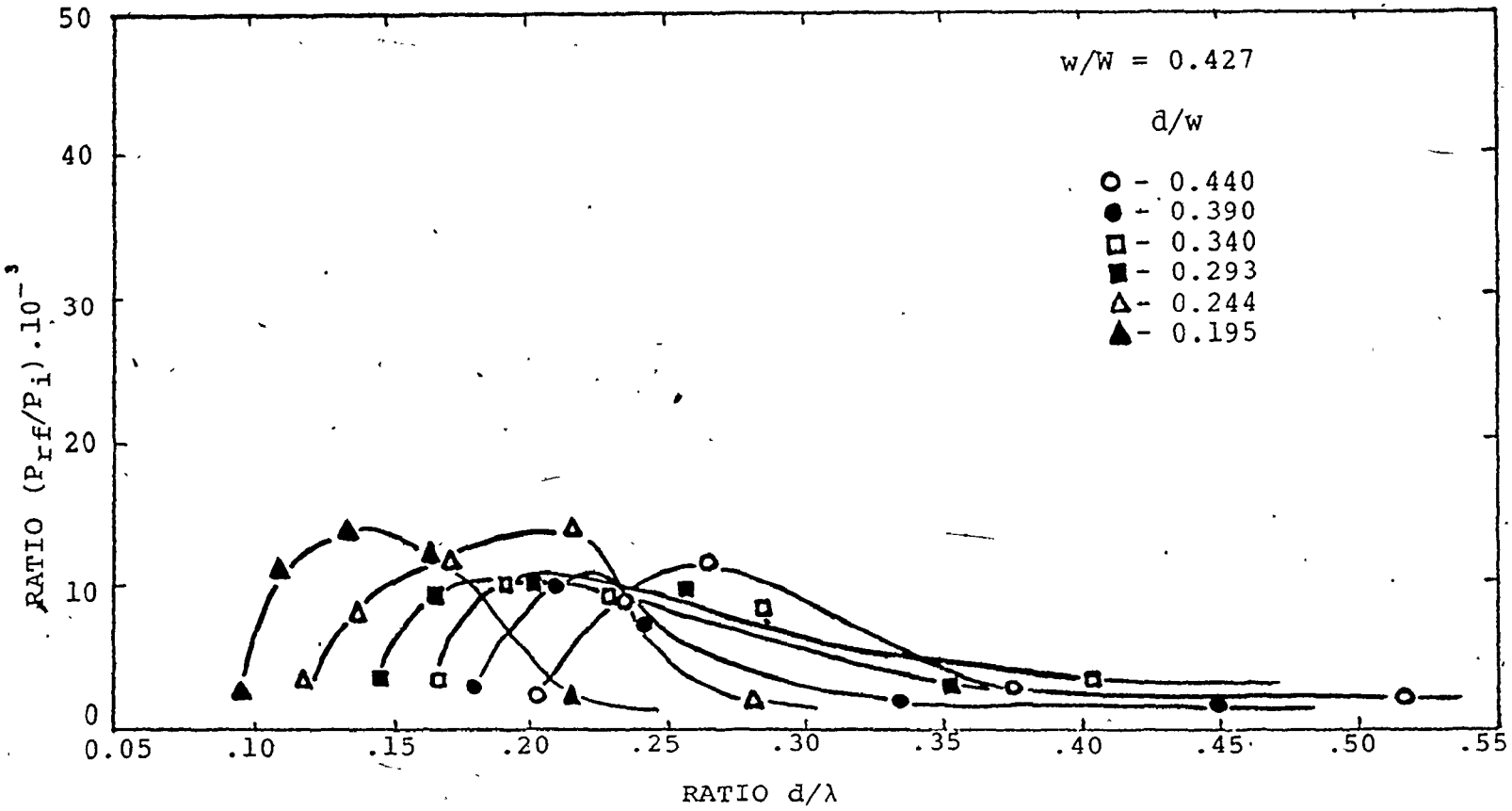

Fig. 5-4 : Power Extraction Coefficient

tested in Figures 5-5 to 5-8.

5.3 Reflectivity

The coefficient of reflection or reflectivity is the ratio of reflected wave amplitude to incident wave amplitude, usually denoted "α":

$$\alpha = \frac{a_r}{a_i} \text{ or } \frac{H_r}{H_i} \tag{4}$$

Unlike "a_t" the accurate evaluation of "a_r" is not straight forward because of the superposition of the reflected wave train on the incident wave train. This produces a partial or full clapotis in which the envelope is characterized by loops and nodes, denoted E_L and E_N as previously outlined in Figure 2-1, providing the wave heights are small enough for linear theory. Once these envelope heights are known the coefficient of reflection is easily obtained from:

$$\alpha = \frac{E_L - E_N}{E_L + E_N} \tag{5}$$

Equation (5) can give rise to serious errors if the waves are steep and non-linear. α is plotted against d/λ for different values of d/w producing curves for each w/W ratio in Figures 5-9 to 5-12.

5.4 Slope of Overflow Ramp

The wave run-up on the resonator overflow flap is essentially similar to wave run-up on any sloping surface. Wave run-up has been studied extensively and it has been

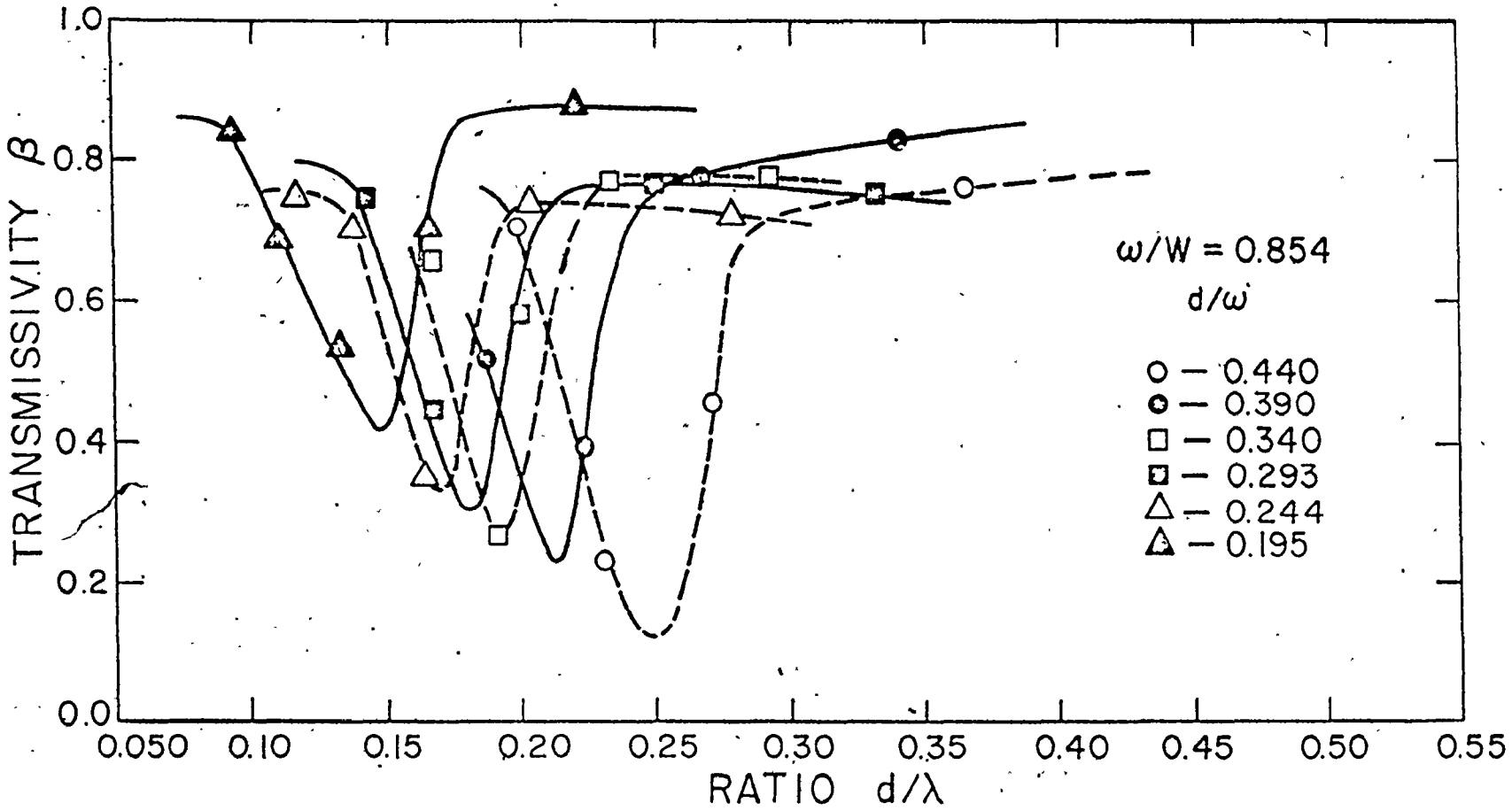

Fig. 5-5 : Transmissivity

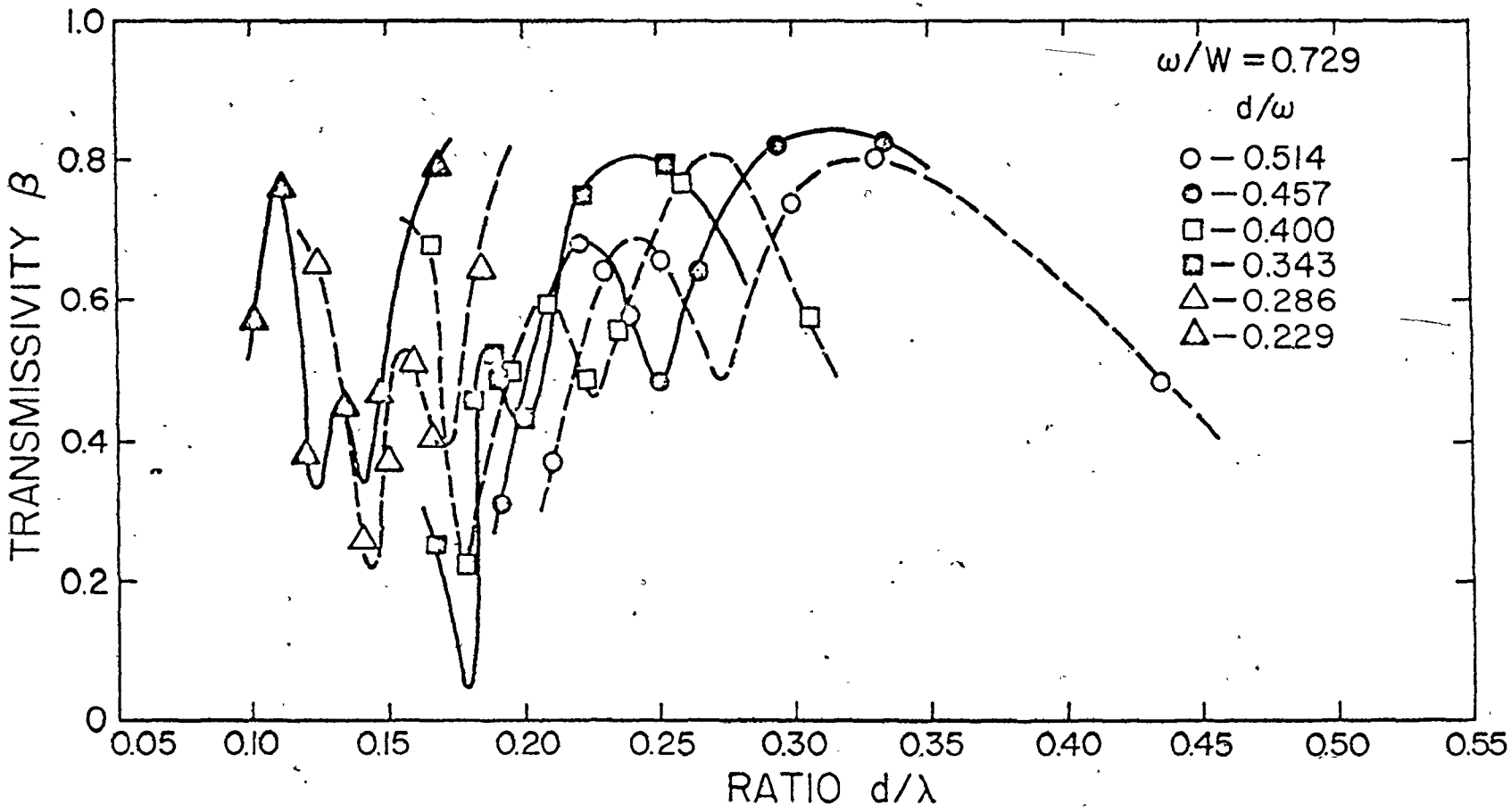

Fig. 5-6 : Transmissivity

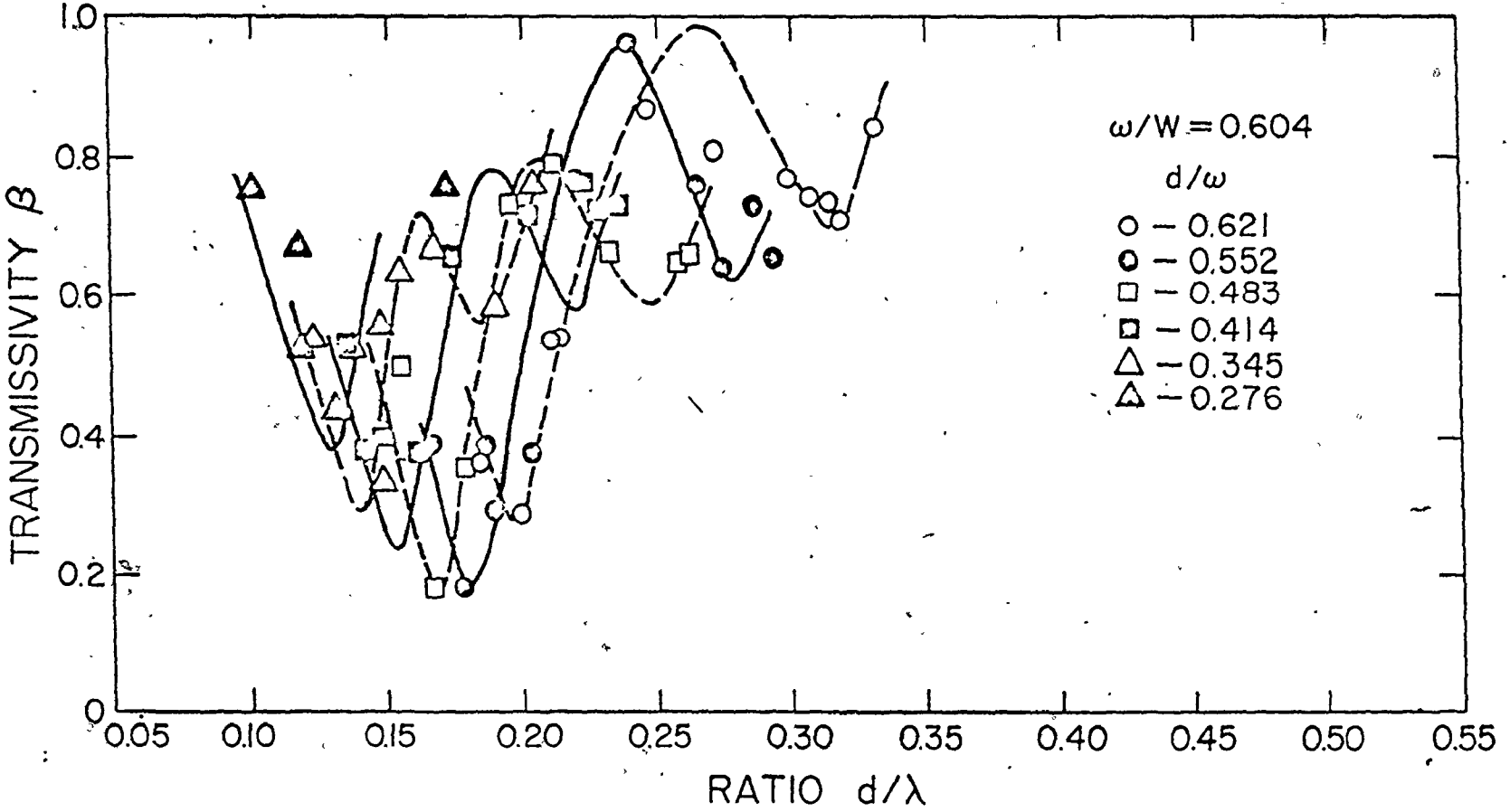

Fig. 5-7 : Transmissivity

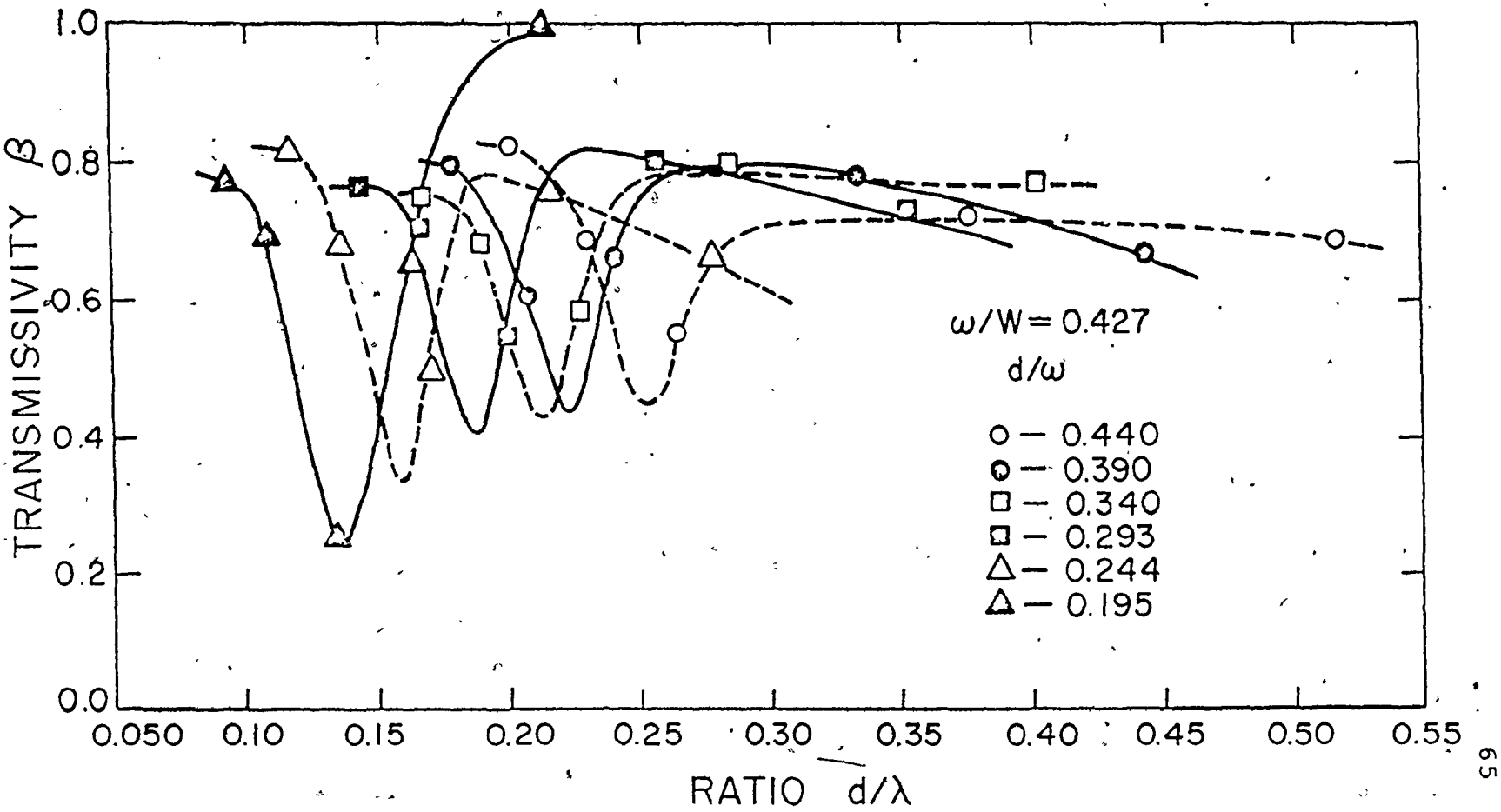

Fig. 5-8 : Transmissivity

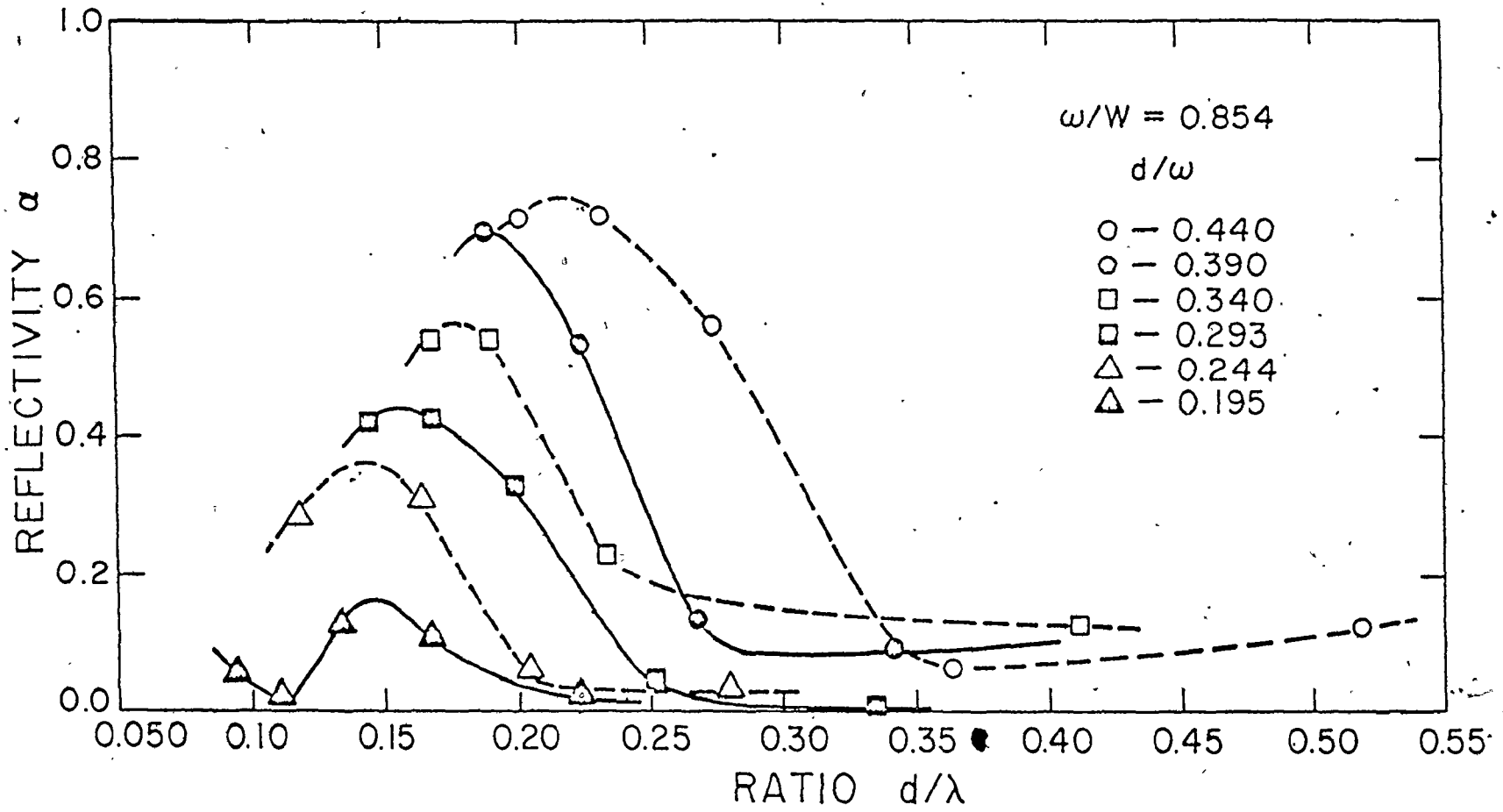

Fig. 5-9 : Reflectivity

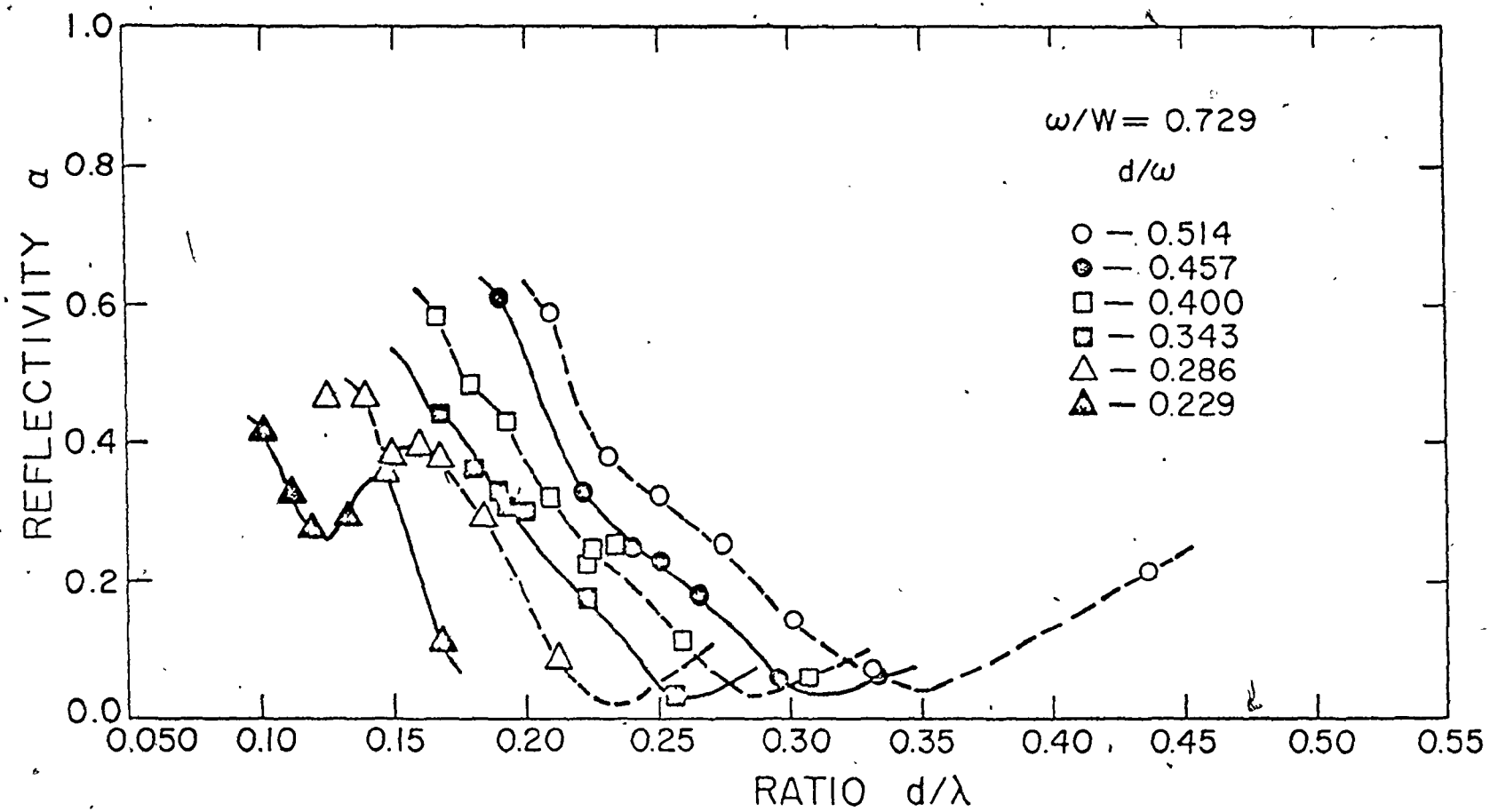

Fig. 5-10 : Reflectivity

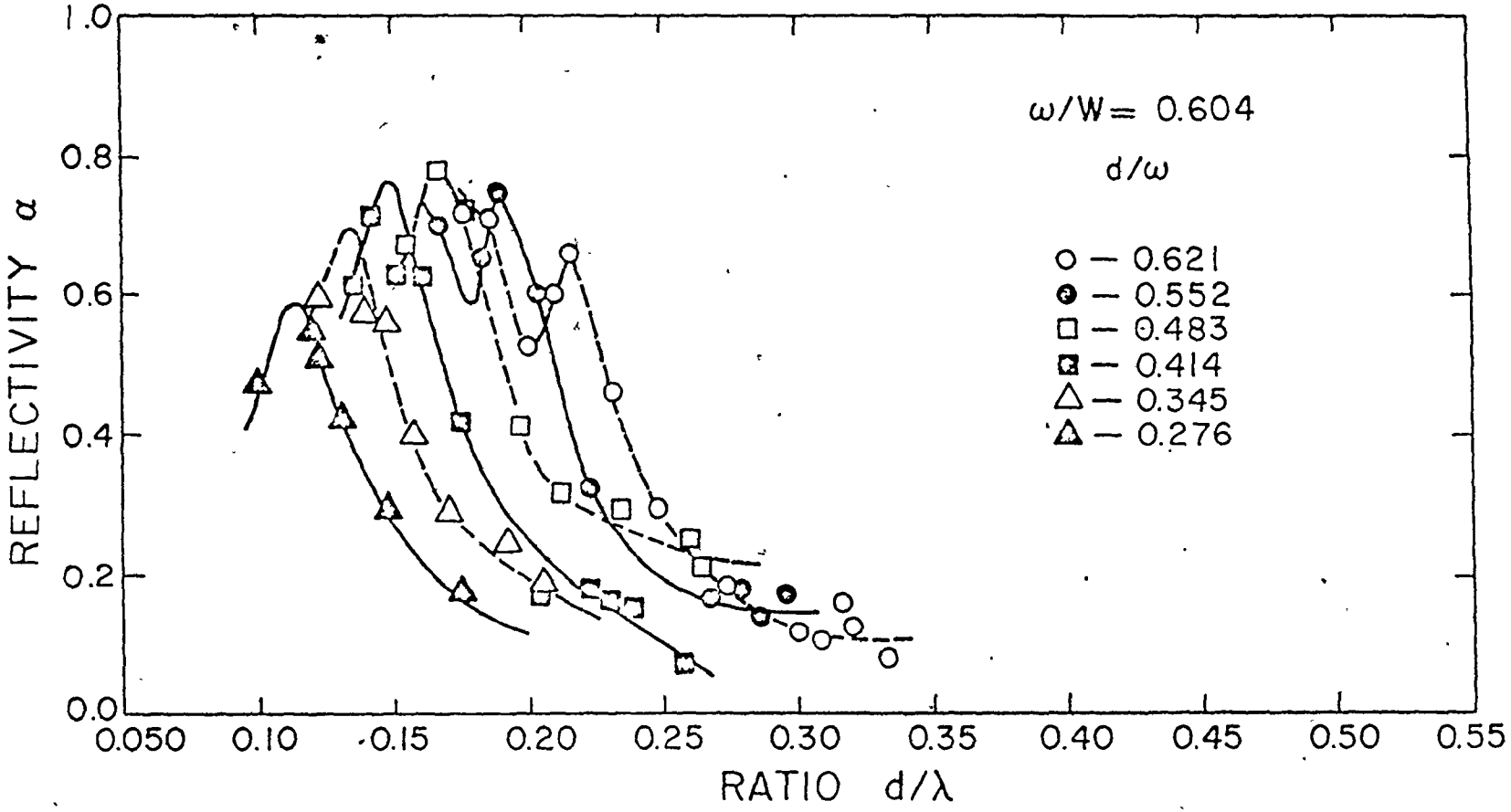

Fig. 5-11 : Reflectivity

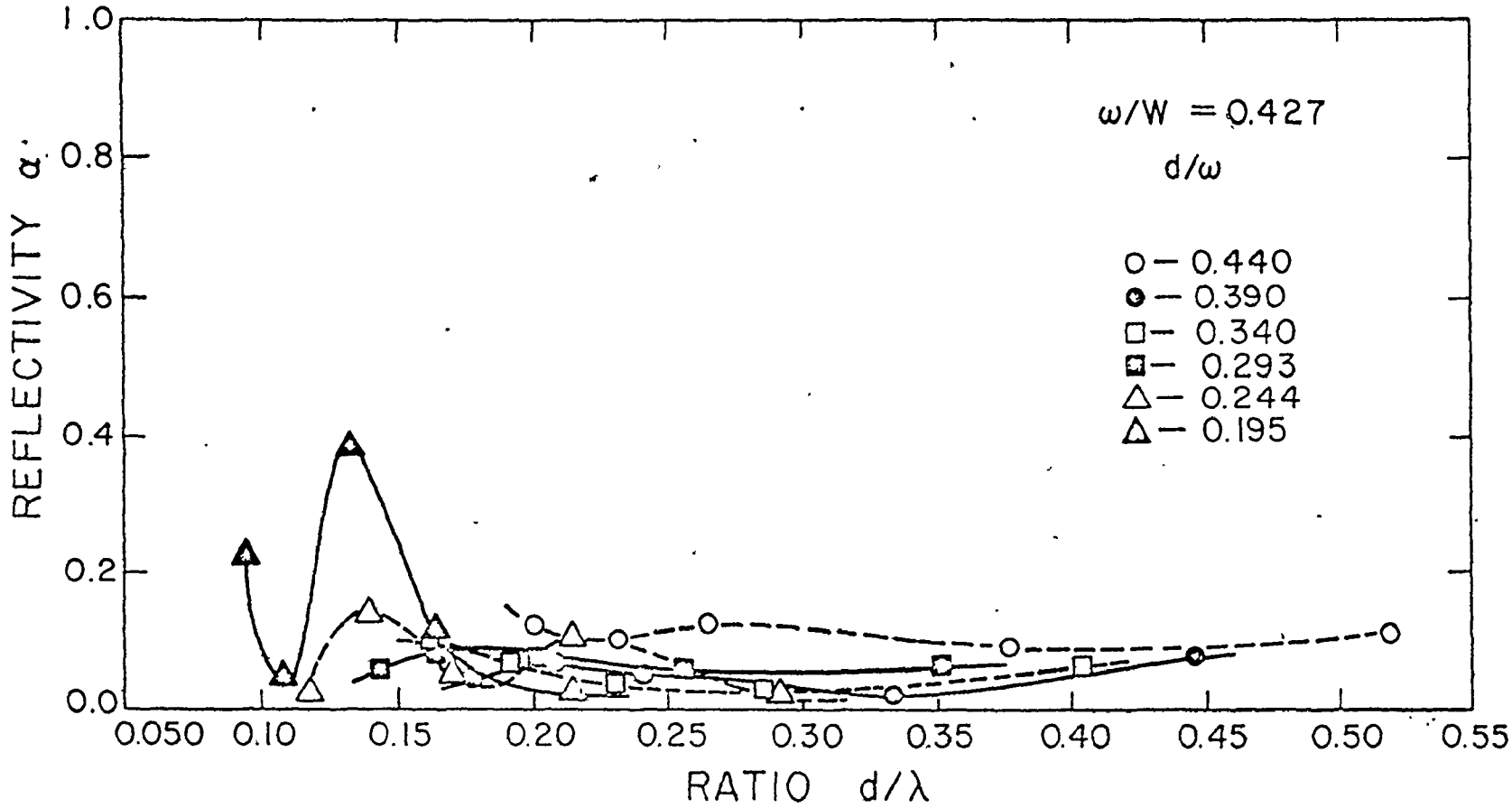

Fig. 5-12 : Reflectivity

found that run-up is a function of both the wave and beach characteristics. In this study factors such as beach porosity, beach roughness, water depth, approach angle and spectral irregularity were either constant or negligible and so overflow angle has been plotted against incident wave steepness in Figure 5-13 for all discharges and Figure 5-14 for maximum discharges.

5.5 Surface Agitation and Streamlines

Because of resonator draw-off there exists a suspicion that small vessels may be drawn into the resonator. Hence both surface agitation and surface flow patterns were observed in the vicinity of the resonator mouth and within the resonator chamber itself. Surface agitation was detected by observing the movements of a floating piece of wood approximately 1 inch by 1/2 inch by 1/8 inch. Surface flow patterns were detected by placing small quantities of a dye solution at various points in the resonator and observing only the trace at the surface. The results of these tests are shown in Figure 5-15 and 5-16, for the two common modes of resonator operation.

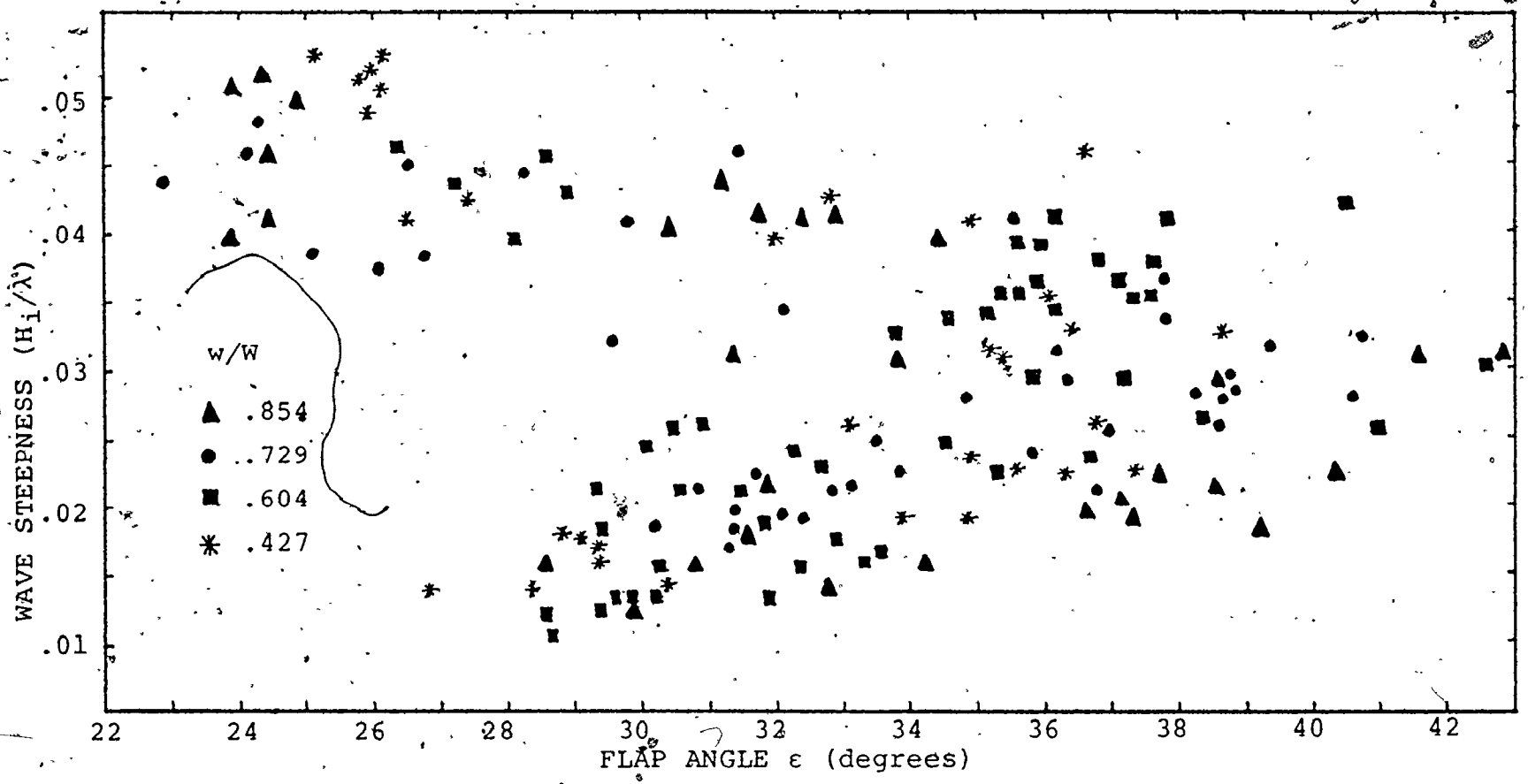

Fig. 5-13 : Overflow Ramp Angle

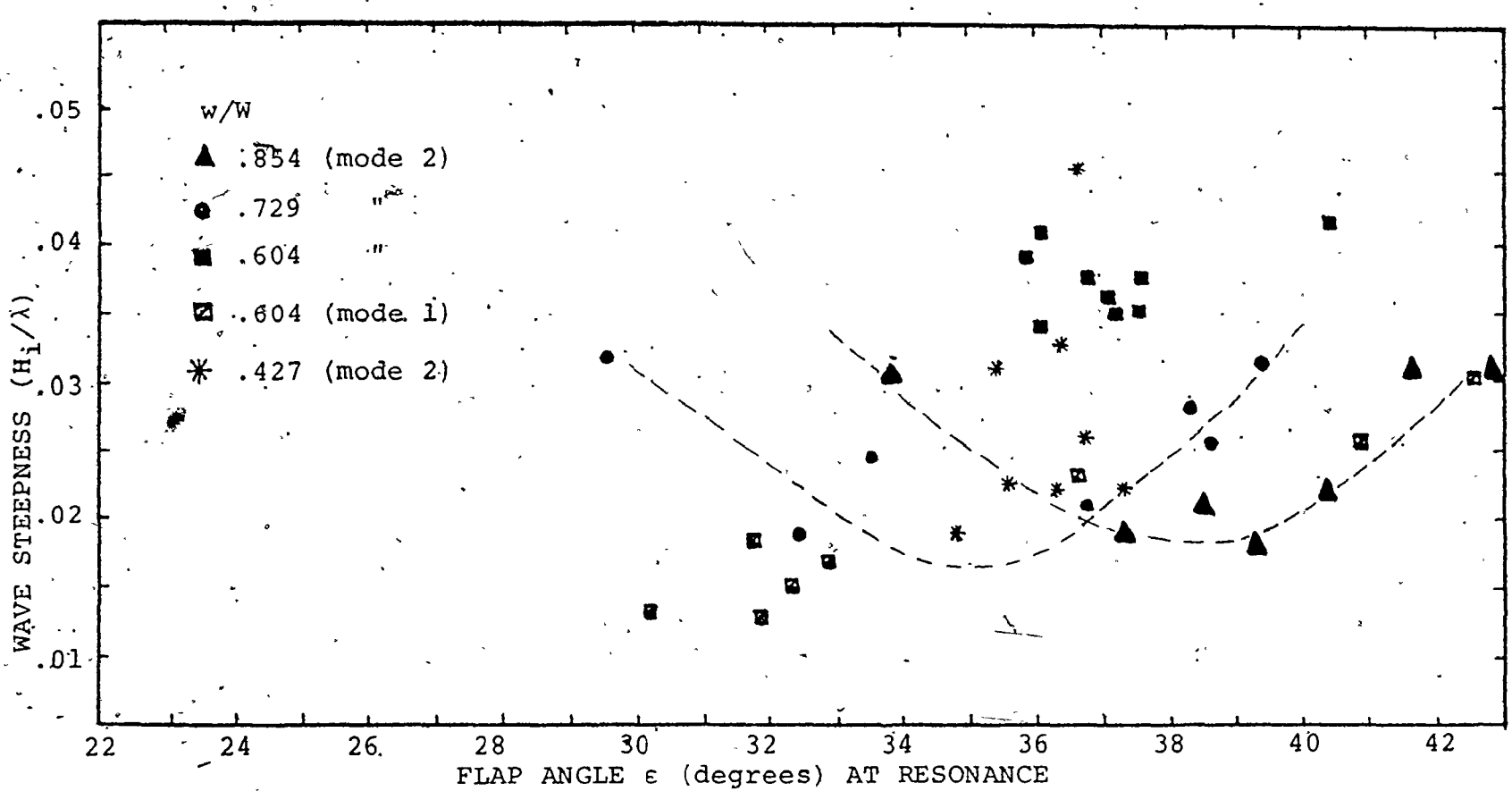

Fig. 5-14 : Overflow Ramp Angle at Resonance

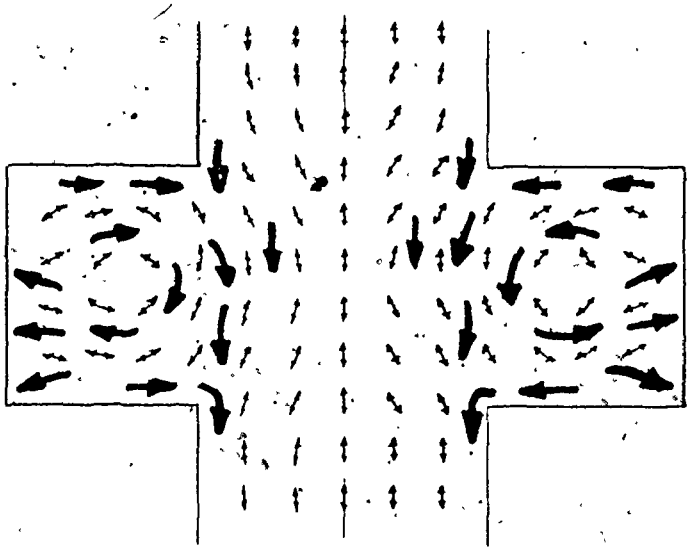

Fig. 5-15 : Surface Agitation and Streamlines Mode 2

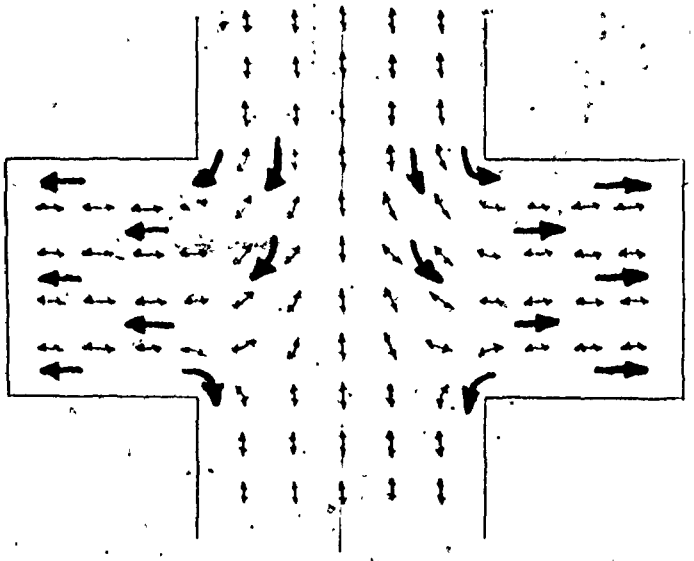

Fig. 5-16 : Surface Agitation and Streamlines Mode 1

CONCLUSIONS

6.1 General Observations

1. General observations may be made regarding the power extraction coefficient curves presented in Figures 5-1 to 5-4. The most significant result, easily observed from the power extraction curves, is that both efficiency and versatility of return flow resonators is very much dependant on the resonator width w. Efficiency decreases with width, and becomes very poor (approx. 1%) for w/W ratios below 0.5

2. The bandwidth for power extraction at a given efficiency is also dependant on resonator width. The narrower the resonator, the finer the tuning for given power extraction, as illustrated by the narrow response curves in Figure 5-3.

3. Peak power extraction tends to increase for decreasing d/w. In other words, the best resonator configuration for power extraction occurs for small values of d. Thus from the experimental results obtained in this study it is evident that the most effective resonator geometry for return flow is the channel expansion configuration. Fortunately this geometry is also the most economical, due to the reduced lengths of breakwater

required. Channel expansion resonators are probably more easily adapted to existing harbour entrances.

4. From the experimental results, between 2 and 5 percent of incident wave power might be obtained for return flow. This probably represents a significant quantity of inexhaustable energy for dredging purposes.

5. When equation (56), page 26, was checked against experimental discharges it yielded flows which were generally an order of magnitude too large. This might be explained by the absence of any energy loss terms in it's derivation. This suggests a significant energy dissipation in the operation of the resonator or overflow ramp. No attempt was made to account for this energy loss.

6. Parameters for peak return flow, in some cases, did not coincide with the design curve, Figure 1-3, presented by James; the values for d/λ obtained in this study being consistently larger. The disagreement increased for increasing resonator depth d and also increased for increasing main channel width W. Insufficient data were available for preparation of a similar design curve for geometry for resonance of return flow resonators.

7. Transmissivity and reflectivity peaks were found to coincide with the return flow peaks. Thus transmissivity minima, reflectivity maxima and return flow power maxima all occur at the same geometries. That is to say, the resonator is working most effectively with

regard to reduction of transmitted waves at the same time as maximum efficiency for return flow is achieved.

8. A general trend in the transmissivity and reflectivity curves suggests that minimum wave transmittance, accompanied by maximum wave reflection, occurs for smaller values of resonant d/λ. This again verifies that the channel expansion configuration is more efficient.

9. During the experiments, the overflow flap in the resonators had to be set manually to obtain the maximum discharge and maximum overflow reservoir height. Thus setting of the flap angle could only be controlled by constantly monitoring the stilling basin water depth. The method was slow and subject to error. Hence the discharges recorded may not have been the absolute maximum possible. The most efficient flap angle was generally observed to occur when a small quantity of water spilled back over the flap into the resonator.

10. Amplitudes in the resonator were, of course, affected by the flap angle. With the flap in a vertical position, maximum amplitudes were obtained; as the flap was lowered increasing the overflow, amplitudes decreased producing a smaller overflow than expected. The flap had to be lowered further until a steady state condition was achieved and at which point some back wash generally occurred. This coincided with maximum levels in the stilling chamber behind the reservoir.

11. From Figure 5-13, page 71, it can be seen that flap angle tended to increase for increasing values of wave steepness and was a maximum for incident wave steepness of approximately 0.03. Regretably there is no well-defined relation evident in Figure 5-13, or Figure 5-14 which shows flap angles at resonance. To some extent, this is to be expected due to the drastic amplification in the resonator chamber. Figures 5-13 and 5-14 are presented here in the hope that they may initiate research.

12. Stilling basin depth increases above the normal still water level varied between the incident wave amplitude and the incident wave height for the geometries tested.

13. Navigability, especially for small craft, in the vicinity of the resonator was of concern in this study. Simple experiments carried out may be noted. The motion of a floating piece of wood 1 inch by 1/2 inch by 1/8 inch was observed carefully. Evidently small craft may experience amplified movement in the junction element, but there appears to be no risk that these small craft will be drawn into the resonator chamber.

14. Observation of streamlines; detected by the addition of a liquid dye solution indicated very small currents entering the resonator. Mode 2 operation experienced a slow rotational motion in the resonator as

indicated in Figure 5-15, page 73. This motion might contribute to an accumulation of floating debris at the "vortex" shown.

15. The highest orbital velocities, accelerations and displacements occur immediately adjacent to the resonator mouth and the curved corner. The bigger the radius of curvature of the corner the slighter will be the vector accelerations. The velocities and displacements appear to be inversely related to the width of the resonator.

In summary general design guidelines may be suggested. The most effective resonator geometry for wave and sediment control appears to be the channel expansion geometry. Such a resonator might employ non-uniform depths in the resonator and main channel to reduce construction costs and also to favorably alter the response of the resonator. A battery configuration employing a common overflow basin might provide protection and scouring flows over a wide range of troublesome wave periods. In any design layout, the resonator or battery should be placed as close to the ocean domain as possible, to reduce the length of entrance adversely affected by the outgoing reflected waves. The agitation provided by the partial clapotis combined with the return flow currents will provide an excellent system of sediment bypassing. This

innovation in harbour resonators has the potential for saving millions of dollars annually in dredging costs as well as preventing severe erosion or accretion of coastal zones by not disrupting the natural littoral sediment transport phenomena.

6.2 Experimental Difficulties

Among the difficulties encountered in the control of the experimental test program was the generation of waves of accurate wave period. This difficulty was overcome by a gear and pulley reduction drive system utilising the rotational inertia of the motor. By timing the waves over a sufficiently long time interval, usually 50 waves, periods were measured to an accuracy of 0.01 seconds.

Transverse oscillations in the tank, occurring at wave periods whose wavelengths were multiples of the tank width initially caused severe deformation in the clapotis envelope. This introduced considerable error over a specific narrow wave frequency band. This problem was overcome by introducing wave guides as described previously into the channel at the nodal points for the highest possible harmonic of the transverse oscillation.

Loop and node heights were found to be slightly time dependent. Envelopes would increase and decrease periodically if the time of observation extended over

a long enough period. This is evidence of long period waves or seiching action in the tank. It was noticed that the envelope minima would decrease while the maxima simultaneously increased. The actual envelope height recorded was the maximum envelope height measured during the periodic variation.

The resonator rear wall had to be reduced in length for each reduction in resonator width. It was initially difficult to place the rear wall in position, due to the rough fit sometimes encountered, without allowing leakage of overflow discharge back into the main channel. Thus the joints between the rear wall and the resonator walls were sealed to reduce this leakage. This condition was aggravated by a sloshing condition set up in the overflow basin. This was overcome by damping this motion in the reservoir with fibreglass screening.

6.3 Expected Prototype Results

The application of these results to full scale return flow resonators is illustrated here.

The prototype harbour will have a width of 120 feet and a depth of 10 feet. The significant wave entering the harbour has a period of 7 seconds and a height of 6 feet. The wavelength associated with this wave period and depth is approximately 120 feet. The ratio w/W should be as high as possible within the constraints

of the local topography. The higher this ratio, the broader the band of wave frequencies that will be affected by the resonator. In this case a value of 0.85 will be used. The corresponding resonator width w is thus approximately 102 feet. The evaluation of the resonator depth d is a trial and error method in which the value of the power extraction coefficient is maximized. The evaluation of d will be condensed here but given to illustrate the method. Firstly, a trial value of d must be chosen. A good first approximation for resonator depth is one third of the resonator width. A first approximation in this example will be 35 feet. Corresponding design parameters are then calculated as being; $d/w \rightarrow 0.343$ and $d/\lambda \rightarrow 0.291$. From Figure 5-1, page 57, the corresponding value of θ is 0.021. Subsequent guesses for the value of d and the resulting values of θ are given below.

For	d = 30.0 ft.	$d/w = 0.294$ $d/\lambda = 0.250$	$\theta = 0.022$
For	d = 25.0 ft.	$d/w = 0.245$ $d/\lambda = 0.208$	$\theta = 0.022$
For	d = 20.0 ft.	$d/w = 0.196$ $d/\lambda = 0.167$	$\theta = 0.015$
For	d = 23.0 ft.	$d/w = 0.225$ $d/\lambda = 0.192$	$\theta = 0.0193$
For	d = 28.0 ft.	$d/w = 0.274$ $d/\lambda = 0.233$	$\theta = 0.0225$

These values may then be plotted as shown in Figure 6-1. The optimum value of d for maximum return flow

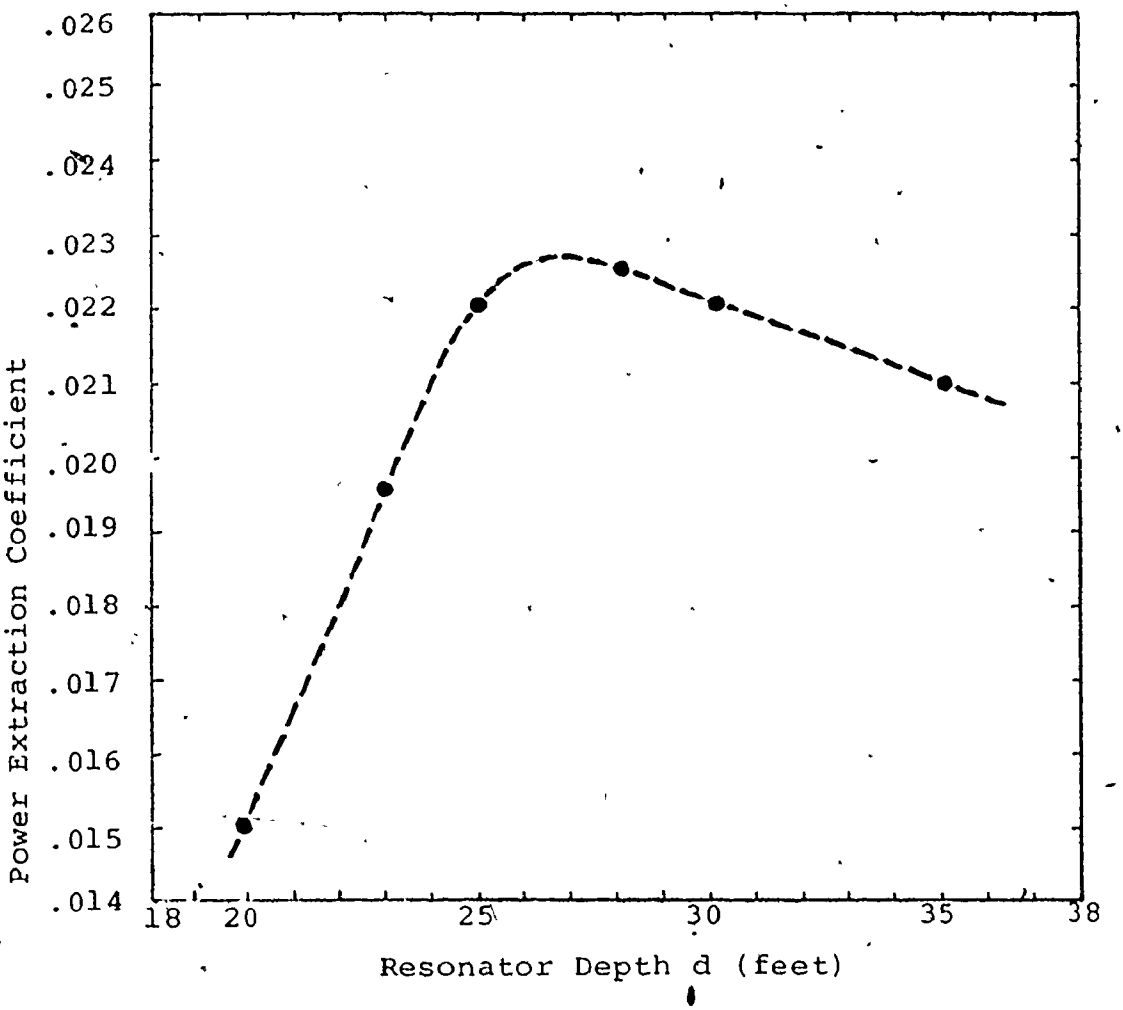

Fig. 6-1 : Resonator depth determination

power may then be evaluated from this plot. In this case a d value of 27 feet gives a power extraction coefficient of approximately 0.0227. The final resonator dimensions are thus, w equal to 102 feet and d equal to 27 feet. Incident wave power is then evaluated using equation 51, page 25 as:

$$P_i = \frac{W\lambda\gamma H_i^2}{8} \cdot C_G$$

$$= \frac{(120)(120)(62.4)(6)^2(15.8)}{8}$$

$$= 6.388 \times 10^7 \text{ ft-lb/sec.}$$

Therefore, power available for return flow is:

$$P_{rf} = 6.388 \times 10^7 \ (0.0227)$$

$$= 1.45 \times 10^6 \text{ ft-lb/sec}$$

or 2,636.8 Horsepower.

Therefore, the product of discharge and stilling basin depth increase for one resonator, from equation 52, page 25, will equal 11,619 ft^4/sec. Now, since stilling basin depth increase was found to generally range between the incident wave amplitude and the incident wave height, a stilling basin depth increase of 4 feet might reasonably be expected. This would yield a return flow discharge of over 2,900 cubic feet per second. The orbital bed motions from the wave clapotis will be amplified and instantaneous scour velocities will vary between 10 and 20 feet/second, which is more than ample for moving even coarse gravels. The potential for scour and prevention of sediment

deposition and penetration into the harbour is evidently substantial and return flow resonators appear to provide a very acceptable means of sediment bypassing and control. With the design parameters obtained in the resonator design it is also possible to predict values for both α and β. From figures 5-5 and 5-9 expected values for reflectivity and transmissivity respectively are 0.08 and 0.76 . These values are not near optimum and a new trial resonator could be tried. It should also be noted that in this example the W/λ ratio is 1.0 which is the upper limit for effectiveness of these resonators.

6.4 Possible Use in Canada

The Great Lakes system supports a large commercial fishing fleet, and a large fleet of pleasure craft, based in numerous small harbours which have problems related to the intrusion of storm waves into the inner harbour zone. The use of return flow harbour resonators would evidently provide a sound solution to the problems faced by these small harbours due to their small dimensions, the range of waves generated and the absence of rocky coasts which might hamper construction. Return flow resonators might be used in small coastal harbours provided that the tidal range does not inactivate the rear overflow wall. A variable geometry resonator would be desirable, due to the wide wave energy spectrum experienced in real wave climates.

RECOMMENDATIONS

7.1 Range of Geometries

The range of resonator geometries tested in this study varied between entrance channel expansions (w>d) to branch channels (w<d). The latter geometry proved to be less efficient than the former. A more extensive study of the channel expansion resonator shape is advisable. Fine dimensional resolution with regard to resonator depth "d" is recommended to provide accurate tuning at resonance.

7.2 Acoustic Modeling

The use of acoustic modeling equipment could greatly expedite the extensive study required to perfect the use of resonators and return flow resonators. Acoustic modeling is very inexpensive once the initial monitoring and generating equipment is provided. This method is quick and encorporates much greater frequency control throughout the experiment. Acoustic modeling of the return flow requires development, since the hydraulic results are now available for comparison.

7.3 Prototype Tests

A return flow resonator should be built on one of the Great Lakes minor harbours which experiences both wave and sedimentation problems. The harbour should be easily accessible from an institution which could properly monitor the test facility.

BIBLIOGRAPHY

1. American Society of Civil Engineers - Task Committee on Small Craft Harbours. "Report on Small Craft Harbours", Manuals and Reports on Engineering Practice No. 50. New York, 1969.

2. Buchwald, V.T. and Williams, N.V. Rectangular Resonators on Infinite and Semi-Infinite Channels, School of Mathematics, University of New South Whales, May 1, 1974.

3. Cornick, H.F. Dock and Harbour Engineering - The Design of Docks, Charles Griffin and Co. Ltd., London, 1968.

4. Cornick, H.F. Dock and Harbour Engineering - The Design of Harbours, Charles Griffin and Co. Ltd., London, 1969.

5. Donnelly, P. and MacInnis, I. "Experiences with Self-Dredging Harbour Entrances", Department of Public Works of Canada. Coastal Engineering Volume 11, 1968.

6. Garrett, R. The Damping Effects of Fibreglass Screens on Monochromatic Waves and Simple Wave Spectra, Master of Science Thesis, Queen's University at Kingston, 1970.

7. Gilbert, G., Thompson, D.M. and Brewer, A.J. "Design Curves for Rectangular and Random Wave Generators", Hydraulics Research Station, Wallingford, England, Journal of Hydraulic Research, Volume 9, No. 2, 1971.

8. Hudspeth, R.T. The Effect of a Single Resonant Expansion Chamber on the Propagation of Long Waves in a Channel, Master of Science Thesis in Civil Engineering, University of Washington, 1966.

9. Ippen, A.T. Estuary and Coastline Hydrodynamics, McGraw-Hill Book Co. Inc., New York, 1966, 51-54.

10. James, W. "Approximate Linear Low-Pass Wave Filters", Journal of the Waterways, Harbours and Coastal Division, ASCE, Volume 99, No. WW1, February 1973, 59-68.

11. James, W. "Two Innovations for Improving Harbour Resonators", Journal of the Waterways, Harbours and Coastal Engineering Division, ASCE, Volume 97, No. WW1, Proc. Paper 7871, February 1971, 115-122.

12. James, W. "Response of Rectangular Resonators to Ocean Wave Spectra", Proc. Institution of Civil Engineers, 1971, Volume 48, (January), 51-63.

13. James, W. "Rectangular Resonators for Harbour Entrances", Proc. American Society of Civil Engineers, 1969, Volume 98, (September), 1512-1530.

14. James, W. "An Experimental Study of End Effects for Rectangular Resonators on Narrow Channels", Journal of Fluid Mechanics, 1970, Volume 44, Part 3, 615-621.

15. James, W. "Resolution of Partial Clapotis", ASCE 1970, Volume 96, No. WW1, (February), 167-170.

16. James, W. "Accurate Wave Measurement in the Presence of Reflections", Journal of Institution of Water Engineers, 1969, Volume 23, No. 8, (November), 497-501.

17. James, W. "Spectral Response of Harbour Resonator Configurations", Coastal Engineering, 1970, Volume 111, No. 132, 2181-2193.

18. Lates, M. "Recherches Hydrauliques de Laboratoire sur l'Efficacite de Quelques Types d'Ouvrages de Protection des Petits Ports Maratimes Contre la Penetration des Vagues et des Alluvions Chariees", L'Institut d'etudes et de Recherches Hydrotechniques, Bucarest, Roumanie, 1963.

19. Lean, G.H. "A Simplified Theory of Permeable Wave Absorbers", Journal of Hydraulic Research, Volume 5, No. W1, 1967.

20. LeMehaute, B. "Progressive Wave Absorbers", Journal of Hydraulic Research, Volume 10, No. 2, 1972.

21. Minikin, R.R. Winds, Waves and Marine Structures, Charles Griffin Co. Ltd., London, 1963.

22. Prandle, D. "Wave Resonators for Harbour Protection", The Dock and Harbour Authority, Volume LV, No. 650, (December) 1974.

23. Trengrouse, G.H. "The Effect of Silences of the Melmhottz Resonator Type on Pressure Waves of Finite Amplitude: Single Pressure Pulses", Journal of Mechanical Engineering Science, Volume 16, No. 4, 1974.

24. Unluata, V. and Mei, C.C. "Effect of Entrance Loss on Harbour Oscillations", Journal of Waterways, Harbours and Coastal Engineer Division, Volume 101, No. WW2, 1975, 161-180.

25. Valembois, J. and Birard, C. Les Ouvrages Resonants et Leur Application a la Protection des Ports, Laboratoire National d'Hydraulique de Chatou.

26. White, I.R.P. Investigation of a Self-Dredging Harbour Entrance, Masters Thesis, Queen's University at Kingston, 1964.

27. Wiegel, R.L. Oceanographical Engineering, Prentice Hall Inc., London, 1964.

28. Yalin, M.S. Theory of Hydraulic Models, MacMillan Press Ltd., London, 1971.

APPENDIX

EXPERIMENTAL RESULTS

W - 24"
w - 20.5"

d	T sec.	λ ft.	d/λ	α	β	Q_{rf} ml/sec	h_{sb} in.	P_{rf} 10^{-3}	H_L in.	H_N in.	H_i in.	P_i 10^{-3}	H_t in.	P_t 10^{-3}	θ 10^{-3}
9	.54	1.45	.517	.127	.784	13.83	0.135	0.69	0.894	0.692	0.793	140.3	0.623	86.16	4.89
	.66	2.05	.365	.065	.759	40.00	0.368	5.41	1.058	0.929	0.994	405.1	0.754	233.32	13.35
	.80	2.75	.273	.568	.459	87.60	0.883	28.41	1.573	0.433	1.003	705.8	0.461	149.10	40.25
	.90	3.25	.231	.721	.236	63.93	0.594	13.95	1.292	0.209	0.751	529.5	0.176	29.62	26.34
	1.00	3.74	.201	.710	.387	38.30	0.348	4.90	0.926	0.157	0.542	349.9	0.210	52.37	13.99
8	.53	1.42	.469	.301	.298	9.30	0.111	0.38	0.874	0.469	0.672	97.1	0.201	8.66	3.90
	.64	1.95	.342	.095	.821	41.50	0.388	5.91	1.104	0.912	1.008	381.4	0.828	257.05	15.51
	.75	2.50	.267	.133	.768	43.50	0.401	6.41	1.050	0.803	0.927	506.4	0.712	299.03	12.65
	.84	2.97	.224	.535	.394	65.83	0.614	14.85	1.056	0.320	0.688	380.7	0.271	59.07	38.99
	.96	3.55	.188	.695	.512	56.67	0.531	11.05	1.123	0.202	0.663	480.2	0.339	125.74	23.01
7	.53	1.42	.411	.125	.566	13.16	0.133	0.64	0.796	0.619	0.708	107.8	0.401	34.55	5.96
	.65	2.00	.292	.232	.773	47.00	0.441	7.61	1.050	0.933	0.992	385.9	0.766	230.36	19.72
	.75	2.50	.233	.228	.769	66.67	0.661	16.19	1.069	0.672	0.871	446.9	0.670	264.79	36.21
	.86	3.05	.191	.532	.263	70.00	0.681	17.51	1.035	0.316	0.676	384.2	0.178	26.68	45.57
	.95	3.50	.167	.540	.661	49.50	0.456	8.29	0.930	0.278	0.604	389.8	0.400	170.52	21.27
6	.55	1.50	.333	.003	.744	12.33	0.150	0.68	0.884	0.879	0.882	183.7	0.656	101.75	3.70
	.65	2.00	.250	.046	.762	47.00	0.457	7.89	1.028	0.937	0.983	378.9	0.749	220.25	20.82
	.75	2.50	.200	.336	.574	80.00	0.802	23.56	1.279	0.636	0.958	540.8	0.550	178.11	43.57
	.85	3.00	.167	.426	.445	72.50	0.717	19.09	1.138	0.458	0.798	521.5	0.355	103.21	36.61
	.95	3.50	.143	.419	.741	43.00	0.407	6.43	1.027	0.420	0.724	559.3	0.536	306.97	11.49

W - 24"
w - 20.5"

d	T	λ	d/λ	α	β	Q_{rf}	h_{sb}	P_{rf} 10^{-3}	H_L	H_N	H_i	P_i 10^{-3}	H_t	P_t 10^{-3}	θ 10^{-3}
5	.55	1.50	.278	.034	.724	12.33	0.114	0.52	0.932	0.871	0.902	192.2	0.653	100.66	2.69
	.66	2.05	.203	.063	.739	50.50	0.515	9.55	1.032	0.910	0.971	387.4	0.718	211.51	24.66
	.76	2.55	.163	.312	.349	72.50	0.760	20.24	1.244	0.652	0.948	549.9	0.332	67.24	36.80
	.85	3.00	.139	.184	.712	64.17	0.657	15.48	0.908	0.626	0.767	481.8	0.546	42.56	32.14
	.96	3.55	.117	.282	.744	38.00	0.380	5.30	0.850	0.476	0.663	481.5	0.494	38.91	11.01
4	.55	1.50	.222	.024	.876	4.34	0.131	0.21	0.944	0.899	0.923	200.8	0.807	153.98	1.04
	.65	2.00	.167	.108	.698	39.00	0.421	6.03	1.123	0.903	1.013	402.9	0.708	196.52	14.97
	.75	2.50	.133	.122	.533	47.50	0.490	8.55	1.021	0.798	0.910	487.9	0.485	138.75	17.52
	.86	3.05	.109	.020	.685	39.50	0.417	6.05	0.851	0.817	0.834	585.6	0.572	274.97	10.33
	.96	3.55	.094	.056	.836	25.25	0.295	2.74	0.723	0.646	0.685	513.2	0.573	358.99	5.33

W - 24"
w - 17.5"

d	T	λ	d/λ	α	β	Q_{rf}	h_{sb}	P_{rf} 10^{-3}	H_L	H_N	H_i	P_i 10^{-3}	H_t	P_t 10^{-3}	θ 10^{-3}
9	.60	1.72	.436	.214	.481	9.83	0.126	0.46	1.193	0.773	0.983	290.2	0.473	67.32	1.57
	.70	2.26	.332	.070	.802	17.25	0.197	1.25	1.076	0.935	1.006	495.2	0.807	318.90	2.52
	.80	2.75	.273	.247	.620	64.17	0.603	14.21	1.051	0.634	0.843	498.1	0.523	191.61	28.53
	.75	2.50	.300	.138	.731	39.00	0.336	4.81	1.101	0.833	0.967	551.6	0.707	294.85	8.73
	.85	3.00	.250	.319	.662	46.00	0.413	6.98	1.048	0.540	0.794	516.3	0.526	226.60	13.51
	.90	3.25	.231	.375	.648	49.50	0.454	8.25	1.148	0.522	0.835	655.4	0.541	275.14	12.59
	.96	3.55	.211	.579	.376	47.00	0.440	7.60	1.327	0.354	0.841	773.9	0.316	109.37	9.81
8	.65	2.00	.333	.059	.820	9.20	0.071	0.24	1.093	0.971	1.032	417.7	0.846	280.28	0.57
	.75	2.50	.266	.178	.639	50.80	0.427	7.97	1.227	0.856	1.041	639.7	0.665	260.85	12.45
	.70	2.26	.295	.051	.823	22.00	0.158	1.28	1.084	0.978	1.031	520.5	0.849	352.62	2.45
	.80	2.77	.240	.242	.581	57.00	0.481	10.07	1.030	0.629	0.830	488.9	0.482	165.09	20.59
	.85	3.00	.222	.326	.678	47.00	0.380	6.56	1.030	0.524	0.777	494.5	0.527	227.11	13.27
	.95	3.48	.192	.608	.304	44.50	0.362	5.92	1.215	0.296	0.756	602.5	0.230	55.84	9.82
	.78	2.65	.252	.233	.485	60.63	0.662	14.74	1.081	0.673	0.877	504.5	0.425	118.71	29.22
7	.63	1.91	.305	.058	.579	11.17	0.122	0.50	1.110	0.989	1.050	398.8	0.608	133.64	1.26
	.70	2.26	.258	.103	.765	22.75	0.226	1.89	1.155	0.939	1.047	536.8	0.801	314.17	3.52
	.75	2.50	.233	.251	.562	60.62	0.572	12.74	1.187	0.711	0.949	531.2	0.533	167.58	23.97
	.80	2.77	.210	.317	.595	53.12	0.493	9.62	0.996	0.516	0.756	406.1	0.450	143.90	23.68
	.85	3.00	.194	.426	.500	44.50	0.399	6.52	1.003	0.404	0.704	405.3	0.352	101.19	16.09
	.90	3.25	.179	.473	.226	45.00	0.402	6.64	1.063	0.380	0.722	490.8	0.163	25.06	13.54
	.95	3.48	.167	.582	.677	43.00	0.396	6.25	1.152	0.304	0.728	559.5	0.493	256.56	11.18
	.78	2.63	.222	.224	.495	54.40	0.583	11.65	1.146	0.727	0.937	567.2	0.464	139.24	20.54
	.77	2.60	.224	.247	.510	61.25	0.650	14.62	1.076	0.650	0.863	471.6	0.440	122.59	31.01

W - 24"
w - 17.5"

d	T	λ	d/λ	α	β	Q_{rf}	h_{sb}	P_{rf} 10^{-3}	H_L	H_N	H_i	P_i 10^{-3}	H_t	P_t 10^{-3}	θ 10^{-3}
6	.65	1.97	.254	.023	.790	12.50	0.216	0.99	1.086	1.037	1.062	430.4	0.839	268.91	2.30
	.70	2.25	.222	.171	.746	27.00	0.343	3.40	1.279	0.906	1.093	580.4	0.815	322.60	5.86
	.75	2.50	.200	.308	.429	58.75	0.635	13.70	1.297	0.686	0.992	579.9	0.426	106.80	23.63
	.80	2.77	.180	.359	.460	50.63	0.559	10.40	1.058	0.499	0.779	430.5	0.358	90.78	24.15
	.77	2.62	.191	.309	.487	62.50	0.680	15.61	1.281	0.676	0.979	614.2	0.477	145.64	25.42
	.85	3.00	.167	.432	.251	48.00	0.528	9.31	1.413	0.561	0.987	797.8	0.248	50.17	11.67
	.778	2.63	.190	.325	.526	60.62	0.665	14.81	1.185	0.603	0.894	516.9	0.470	142.57	28.64
5	.65	1.97	.211	.080	.999	16.50	0.282	1.71	1.131	0.963	1.047	419.2	1.250	597.57	4.08
	.70	2.25	.185	.294	.646	47.50	0.555	9.68	1.445	0.789	1.117	606.7	0.722	253.49	15.96
	.75	2.50	.167	.373	.409	59.37	0.660	14.39	1.232	0.562	0.897	474.6	0.367	79.45	30.32
	.80	2.77	.150	.371	.373	55.62	0.626	12.79	1.030	0.472	0.751	400.8	0.280	55.72	31.91
	.845	2.97	.140	.464	.264	52.50	0.605	11.67	1.069	0.391	0.730	428.7	0.193	29.96	27.21
	.925	3.37	.124	.458	.652	39.00	0.464	6.65	1.282	0.476	0.879	771.5	0.573	328.30	8.61
	.77	2.60	.160	.390	.519	58.75	0.659	14.22	1.124	0.493	0.809	413.9	0.420	111.43	34.36
4	.65	1.97	.169	.101	.790	23.75	0.398	3.47	1.200	0.979	1.090	453.5	0.861	283.19	7.66
	.70	2.25	.148	.352	.466	50.62	0.635	11.81	1.345	0.645	0.995	481.4	0.464	104.69	24.52
	.845	2.97	.112	.323	.767	46.87	0.598	10.29	0.984	0.503	0.743	444.5	0.570	261.34	23.16
	.90	3.25	.102	.417	.578	28.67	0.430	4.53	1.101	0.453	0.777	569.3	0.449	190.08	7.95
	.75	2.50	.133	.288	.449	60.62	0.728	16.21	1.251	0.692	0.972	556.7	0.436	111.87	29.11
	.805	2.80	.119	.269	.387	59.37	0.728	15.87	1.182	0.680	0.931	627.1	0.360	93.50	25.31

W - 24"
w - 14.5"

d	T	λ	d/λ	α	β	Q_{rf}	h_{sb}	P_{rf} 10^{-3}	H_L	H_N	H_i	P_i 10^{-3}	H_t	P_t 10^{-3}	θ 10^{-3}
9	.70	2.26	.332	.076	.834	23.50	0.276	2.38	1.164	0.999	1.082	572.7	0.902	398.39	4.16
	.75	2.50	.300	.111	.765	50.62	0.516	9.59	1.129	0.904	1.017	609.5	0.778	356.58	15.74
	.80	2.75	.273	.177	.804	35.00	0.368	4.73	1.006	0.703	0.855	512.3	0.687	331.13	9.23
	.855	3.03	.248	.290	.861	29.67	0.320	3.49	1.001	0.551	0.776	501.1	0.668	371.31	6.96
	.90	3.25	.231	.456	.708	30.33	0.327	3.64	0.976	0.365	0.671	423.9	0.475	212.29	8.59
	.95	3.48	.216	.652	.535	34.16	0.355	4.45	0.940	0.198	0.569	263.8	0.305	75.54	16.89
	1.00	3.75	.200	.517	.285	45.50	0.478	7.99	1.180	0.376	0.778	725.4	0.222	59.07	11.01
	1.05	4.00	.187	.703	.385	26.11	0.294	2.82	0.838	0.146	0.492	322.1	0.190	47.79	8.75
	.96	3.55	.211	.597	.534	33.75	0.360	4.46	0.963	0.243	0.603	398.3	0.322	113.56	11.21
	.713	2.34	.320	.130	.709	60.00	0.595	13.11	1.183	0.910	1.047	571.9	0.742	287.51	22.93
	.733	2.43	.308	.100	.740	56.25	0.572	11.82	1.129	0.924	1.027	589.7	0.760	322.84	20.04
	.725	2.37	.316	.167	.734	55.63	0.571	11.67	1.131	0.808	0.970	501.9	0.712	270.73	23.24
8	.70	2.26	.295	.171	.651	47.50	0.554	9.67	1.261	0.892	1.077	567.5	0.701	240.28	17.03
	.73	2.40	.278	.176	.622	53.75	0.622	12.28	1.190	0.834	1.012	560.5	0.630	216.88	21.91
	.75	2.50	.267	.164	.758	47.50	0.554	9.67	1.225	0.880	1.053	653.4	0.798	375.64	14.79
	.80	2.75	.242	.294	.960	28.00	0.383	3.94	1.129	0.616	0.873	534.1	0.837	491.51	7.38
	.85	3.00	.222	.320	.764	26.33	0.369	3.57	1.019	0.525	0.772	488.1	0.590	284.61	7.31
	.90	3.25	.205	.597	.371	35.00	0.432	5.55	1.481	0.374	0.928	811.1	0.344	111.58	6.85
	.95	3.50	.190	.739	.289	38.50	0.457	6.46	1.248	0.187	0.718	550.1	0.208	46.00	11.75
	1.05	4.00	.167	.692	.385	15.00	0.296	1.64	0.824	0.150	0.487	315.6	0.188	46.78	5.18
	1.00	3.75	.178	.713	.179	30.00	0.422	4.65	1.178	0.197	0.688	566.5	0.123	18.13	8.21
	.973	3.60	.185	.648	.366	20.00	0.333	2.45	0.926	0.198	0.562	354.1	0.206	47.35	6.91
	.715	2.32	.287	.135	.727	54.37	0.611	12.20	1.125	0.857	0.991	505.0	0.720	266.58	24.16
7	.70	2.26	.258	.241	.645	51.25	0.609	11.46	1.188	0.726	0.957	448.5	0.617	186.41	25.56
	.75	2.50	.233	.295	.656	40.00	0.492	7.23	1.272	0.693	0.983	569.4	0.645	245.03	12.69
	.80	2.75	.212	.312	.784	21.00	0.352	2.72	1.073	0.563	0.818	469.5	0.643	288.72	5.78
	.845	2.96	.197	.441	.726	29.00	0.403	4.29	1.057	0.410	0.734	430.5	0.533	226.86	9.97
	.90	3.25	.179	.718	.349	31.67	0.432	5.03	1.047	0.172	0.610	350.3	0.213	42.58	14.35

W - 24"
w - 14.5"

d	T	λ	d/λ	α	β	Q_{rf}	h_{sb}	P_{rf} 10^{-3}	H_L	H_N	H_i	P_i 10^{-3}	H_t	P_t 10^{-3}	θ 10^{-3}
7	.95	3.50	.167	.776	.177	31.00	0.422	4.81	0.977	0.123	0.550	323.2	0.098	10.16	14.87
	1.00	3.75	.156	.662	.494	35.42	0.473	6.15	1.255	0.255	0.755	683.1	0.373	166.74	9.01
	.69	2.22	.263	.211	.653	53.13	0.632	12.33	1.351	0.881	1.116	590.7	0.729	252.05	20.87
6	.64	1.95	.256	.060	.281	12.00	0.210	0.93	1.144	1.015	1.080	435.7	0.304	34.44	2.12
	.695	2.24	.223	.172	.760	52.50	0.565	10.89	1.245	0.880	1.063	544.1	0.808	314.25	20.02
	.741	2.46	.203	.159	.707	50.00	0.537	9.86	1.170	0.849	1.010	582.6	0.714	291.42	16.93
	.82	2.85	.175	.401	.651	52.50	0.557	10.74	1.430	0.612	1.021	779.5	0.665	330.69	13.78
	.87	3.10	.161	.619	.370	55.00	0.589	11.90	1.402	0.330	0.866	649.6	0.320	88.69	18.32
	1.02	3.85	.136	.605	.525	28.67	0.347	3.65	1.005	0.247	0.626	492.0	0.329	135.47	7.43
	.955	3.53	.142	.702	.377	27.00	0.327	3.24	0.926	0.162	0.544	321.0	0.205	45.58	10.10
	.92	3.35	.149	.625	.390	49.50	0.541	9.84	1.482	0.342	0.912	823.2	0.356	125.43	11.95
	.67	2.10	.238	.156	.722	23.75	0.302	2.63	1.239	0.904	1.072	492.1	0.774	256.77	5.35
	.685	2.18	.230	.167	.712	52.50	0.569	10.97	1.248	0.891	1.070	524.9	0.762	266.44	20.90
5	.655	2.03	.205	.176	.757	26.33	0.293	2.83	1.291	0.904	1.098	486.1	0.831	278.34	5.83
	.685	2.18	.191	.243	.582	70.80	0.721	18.76	1.369	0.834	1.102	556.7	0.642	188.84	33.69
	.741	2.46	.169	.281	.666	55.00	0.550	11.11	1.346	0.756	1.051	631.4	0.700	279.71	17.60
	.788	2.67	.156	.390	.636	50.63	0.517	9.61	1.097	0.481	0.789	413.8	0.502	167.51	23.23
	.854	3.02	.138	.565	.520	61.88	0.609	13.84	1.588	0.442	1.015	852.8	0.528	230.76	16.23
	.932	3.40	.123	.588	.540	41.00	0.414	6.23	1.192	0.309	0.751	572.6	0.405	166.75	10.89
	.812	2.80	.149	.568	.336	78.33	0.803	23.10	1.618	0.446	1.032	771.5	0.347	86.97	29.94
4	.634	1.93	.173	.166	.752	25.00	0.239	2.19	1.176	0.842	1.009	376.8	0.759	212.91	5.82
	.693	2.23	.149	.302	.554	65.83	0.620	14.99	1.316	0.706	1.011	488.9	0.560	150.01	30.66
	.76	2.55	.131	.431	.435	60.00	0.565	12.45	1.598	0.635	1.117	763.1	0.486	144.17	16.32
	.813	2.80	.119	.539	.669	70.00	0.648	16.66	1.391	0.417	0.904	592.0	0.605	265.14	28.14
	.91	3.27	.102	.464	.751	50.00	0.447	8.21	1.297	0.475	0.886	745.3	0.666	420.48	11.02
	.807	2.77	.120	.500	.524	78.33	0.739	21.26	1.321	0.440	0.881	550.7	0.461	150.95	38.61

W - 48"
w - 20.5"

d	T	λ	d/λ	α	β	Q_{rf}	h_{sb}	P_{rf} 10^{-3}	H_L	H_N	H_i	P_i 10^{-3}	H_t	P_t 10^{-3}	θ 10^{-3}
9	.54	1.45	.517	.110	.681	15.90	0.158	0.92	1.041	0.835	0.938	392.5	0.639	181.87	2.35
	.65	2.00	.375	.090	.718	26.67	0.246	2.41	1.118	0.934	1.026	825.6	0.737	426.03	2.92
	.82	2.85	.263	.124	.552	63.34	0.597	13.89	1.005	0.783	0.894	1196.8	0.494	364.69	11.60
	.90	3.25	.231	.096	.692	52.50	0.494	9.53	0.812	0.670	0.741	1034.3	0.513	495.72	9.21
	1.00	3.74	.201	.118	.814	25.00	0.230	2.11	0.735	0.580	0.658	1031.7	0.536	684.33	2.05
8	.55	1.50	.444	.076	.665	14.87	0.189	1.03	1.008	0.866	0.937	415.2	0.623	183.54	2.49
	.65	2.00	.333	.017	.777	18.67	0.217	1.49	1.010	0.976	0.993	774.3	0.772	467.36	1.92
	.80	2.75	.242	.048	.656	45.45	0.463	7.73	0.915	0.831	0.873	1069.4	0.573	460.71	7.23
	.89	3.20	.208	.055	.604	52.75	0.523	10.13	0.784	0.702	0.743	1010.5	0.449	369.01	10.03
	1.00	3.74	.178	.041	.793	26.93	0.288	2.85	0.681	0.627	0.654	1021.8	0.519	643.47	2.79
7	.54	1.45	.402	.060	.769	16.50	0.199	1.21	0.986	0.875	0.931	386.3	0.716	228.70	3.12
	.66	2.05	.284	.027	.785	42.00	0.424	6.54	0.994	0.941	0.968	769.2	0.760	473.99	8.50
	.76	2.55	.229	.041	.575	53.12	0.546	10.65	1.007	0.927	0.967	1143.3	0.557	378.65	9.32
	.86	3.05	.191	.065	.678	56.63	0.579	12.04	0.878	0.771	0.825	1144.7	0.559	526.16	10.52
	.95	3.50	.167	.090	.747	29.67	0.314	3.42	0.784	0.654	0.719	1104.7	0.538	617.39	3.10
6	.53	1.42	.352	.053	.721	18.34	0.192	1.29	0.943	0.848	0.896	344.9	0.646	179.49	3.75
	.64	1.95	.256	.049	.799	45.50	0.454	7.59	1.044	0.946	0.995	743.3	0.796	475.11	10.21
	.75	2.50	.200	.064	.543	55.00	0.544	10.99	0.992	0.873	0.933	1025.4	0.507	302.51	10.72
	.86	3.05	.164	.081	.708	56.67	0.557	11.59	0.908	0.772	0.840	1188.1	0.595	596.11	9.76
	.95	3.50	.143	.055	.762	33.34	0.324	3.97	0.761	0.682	0.722	1112.4	0.550	646.44	3.57
5	.55	1.50	.278	.035	.650	9.00	0.197	0.65	0.939	0.876	0.908	389.9	0.590	164.61	1.67
	.64	1.95	.214	.103	.755	57.50	0.592	12.50	1.188	0.966	1.077	871.3	0.814	497.13	14.35
	.74	2.45	.170	.047	.491	56.67	0.582	12.11	1.002	0.912	0.957	1040.4	0.470	250.94	11.64
	.86	3.05	.137	.141	.681	50.83	0.527	9.84	0.995	0.749	0.872	1280.3	0.594	593.11	7.68
	.96	3.55	.117	.017	.815	32.00	0.323	3.80	0.698	0.674	0.686	1030.9	0.559	684.52	3.68

W - 48"
w - 20.5"

d	T	λ	d/λ	α	β	Q_{rf}	h_{sb}	P_{rf} 10^{-3}	H_L	H_N	H_i	P_i 10^{-3}	H_t	P_t 10^{-3}	θ 10^{-3}
4	.56	1.56	.214	.035	.999	14.00	0.185	0.95	0.938	0.874	0.906	416.2	0.923	431.46	2.29
	.66	2.05	.163	.107	.657	51.00	0.524	9.82	1.103	0.890	0.997	815.9	0.655	352.53	12.03
	.75	2.50	.133	.381	.251	64.17	0.658	15.51	1.335	0.598	0.967	1101.0	0.243	69.60	14.08
	.86	3.05	.109	.039	.693	59.17	0.610	13.26	0.856	0.792	0.824	1143.3	0.571	548.99	11.60
	.96	3.55	.094	.221	.769	26.67	0.306	2.99	0.887	0.566	0.727	1156.2	0.559	683.29	2.59

W	w	d	T	WAVE STEEPNESS	FLAP ANGLE
24	20.5	9	0.54	.0456	24.45
			.66	.0404	30.48
			.80	.0304	45.49
			.90	.0193	36.69
			1.00	.0121	29.95
		8	.53	.0394	23.85
			.64	.0431	31.01
			.75	.0309	31.36
			.84	.0193	37.27
			.96	.0156	34.92
		7	.53	.0416	24.41
			.65	.0413	32.44
			.75	.0290	38.64
			.86	.0185	39.23
			.95	.0144	32.85
		6	.55	.0490	24.83
			.65	.0410	32.87
			.75	.0319	42.91
			.85	.0222	40.30
			.95	.0172	31.52
		5	.55	.0501	23.93
			.66	.0395	34.47
			.76	.0310	41.61
			.85	.0213	38.52
			.96	.0156	30.80
		4	.55	.0513	24.35
			.65	.0422	31.89
			.75	.0303	33.78
			.86	.0228	31.79
			.96	.0161	28.55

W	w	d	T	WAVE STEEPNESS	FLAP ANGLE
24	17.5	9	0.60	.0476	24.23
			.70	.0371	26.03
			.80	.0255	36.96
			.75	.0322	29.63
			.85	.0220	31.68
			.90	.0214	32.79
			.96	.0197	32.41
		8	.65	.0430	22.85
			.75	.0347	32.06
			.70	.0380	25.04
			.80	.0250	33.53
			.85	.0216	30.80
			.95	.0181	30.32
			.78	.0276	38.67
		7	.63	.0458	24.13
			.70	.0386	26.77
			.75	.0316	36.07
			.80	.0227	33.86
			.85	.0196	31.31
			.90	.0185	31.38
			.95	.0174	31.22
			.78	.0297	36.38
			.77	.0277	38.32
		6	.65	.0449	26.51
			.70	.0405	29.81
			.75	.0331	37.88
			.80	.0234	35.70
			.77	.0311	39.20
			.85	.0274	34.83
			.78	.0283	38.75
		5	.65	.0443	28.21
			.70	.0414	35.59
			.75	.0299	38.61
			.80	.0226	37.62
			.84	.0205	37.01
			.93	.0217	33.06
			.77	.0259	38.58
		4	.65	.0461	31.28
			.70	.0369	37.88
			.84	.0209	36.81
			.90	.0199	32.14
			.75	.0324	40.63
			.81	.0277	40.63

W	w	d	T	WAVE STEEPNESS	FLAP ANGLE
24	14.5	9	0.70	.0399	.28.06
			.75	.0339	34.50
			.80	.0259	30.47
			.85	.0213	29.21
			.90	.0172	29.39
			.95	.0136	30.13
			1.00	.0173	33.45
			1.05	.0102	28.53
			.96	.0141	30.26
			.71	.0373	36.73
			.73	.0352	36.07
			.72	.0341	36.04
		8	.70	.0397	35.56
			.73	.0351	37.50
			.75	.0351	35.56
			.80	.0264	30.88
			.85	.0214	30.50
			.90	.0238	32.19
			.95	.0171	32.87
			1.05	.0101	28.61
			1.00	.0153	31.92
			.97	.0130	29.55
			.72	.0356	37.18
		7	.70	.0353	37.13
			.75	.0328	33.83
			.80	.0248	30.05
			.85	.0207	31.41
			.90	.0156	32.19
			.95	.0131	31.92
			1.00	.0168	33.31
			.69	.0419	37.79
		6	.64	.0462	26.36
			.69	.0395	35.87
			.74	.0342	35.08
			.82	.0298	35.65
			.87	.0233	36.55
			1.02	.0135	29.92
			.95	.0128	29.39
			.92	.0227	35.20
			.67	.0425	28.74
			.68	.0409	35.99

W	w	d	T	WAVE STEEPNESS	FLAP ANGLE
24	14.5	5	0.65	.0451	28.50
			.68	.0421	40.42
			.74	.0356	35.45
			.79	.0246	34.53
			.85	.0280	37.13
			.93	.0184	31.71
			.81	.0307	42.94
		4	.63	.0436	27.10
			.69	.0378	37.44
			.76	.0365	35.87
			.81	.0269	38.26
			.91	.0226	32.60
			.80	.0265	40.97

W	w	d	T	WAVE STEEPNESS	FLAP ANGLE
48	20.5	9	0.54	.0539	25:04
			.65	.0428	27.28
			.82	.0261	36.78
			.90	.0190	33.89
			1.00	.0147	26.87
		8	.55	.0521	25.82
			.65	.0414	26.54
			.80	.0264	33.04
			.89	.0194	34.69
			1.00	.0146	28.37
		7	.54	.0535	26.08
			.66	.0394	31.98
			.76	.0316	35.34
			.86	.0225	36.27
			.95	.0171	29.05
		6	.53	.0526	25.90
			.64	.0425	32.79
			.75	.0311	35.28
			.86	.0229	35.64
			.95	.0172	29.31
		5	.55	.0504	26.03
			.64	.0460	36.64
			.74	.0325	36.35
			.86	.0238	34.81
			.96	.0161	29.29
		4	.56	.0484	25.72
			.66	.0405	34.72
			.75	.0322	38.55
			.86	.0225	37.16
			.96	.0171	28.84

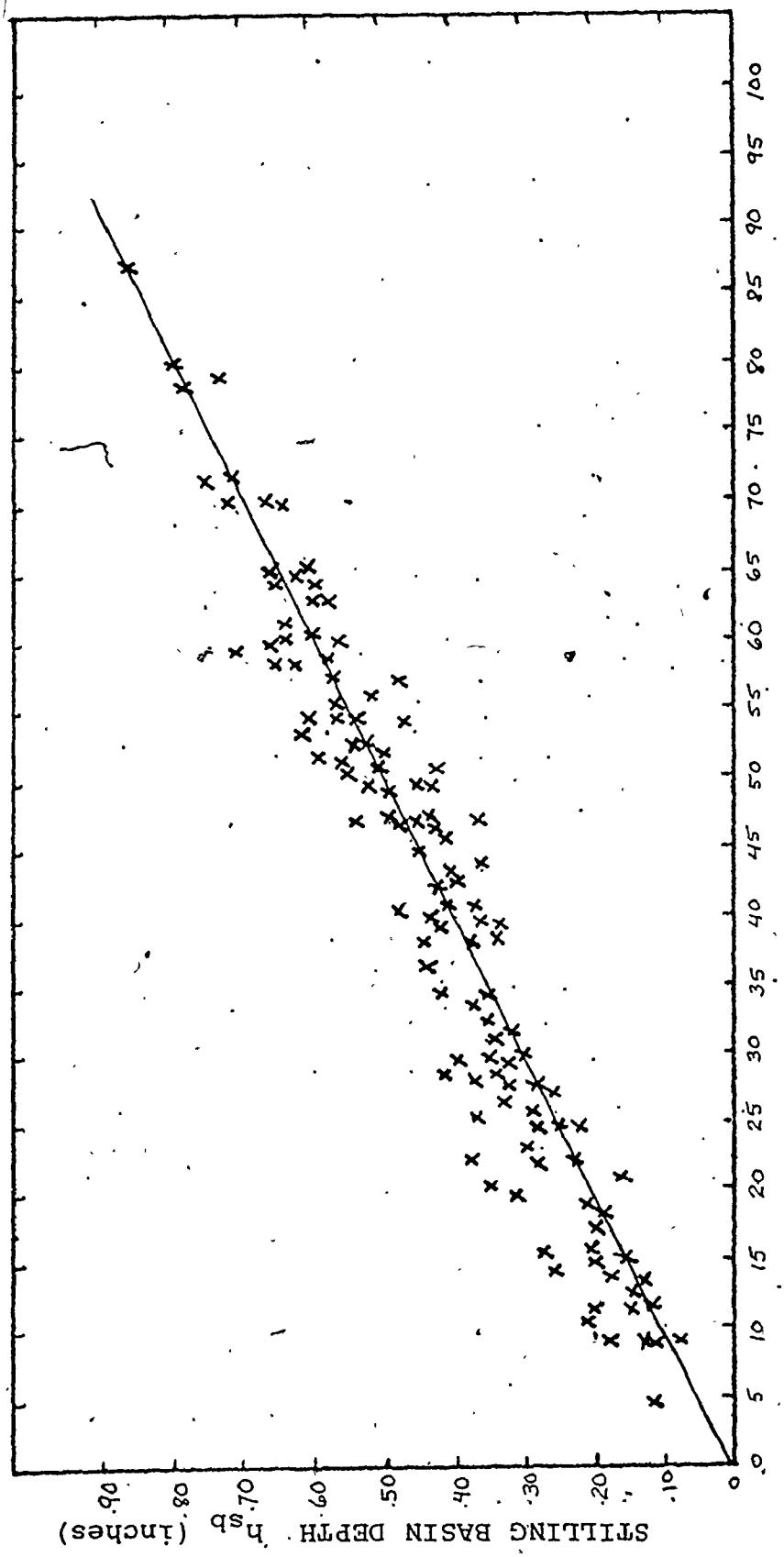
STILLING BASIN DEPTH h_{sb} (inches)
.10
.20
.30
.40
.50
.60
.70
.80
.90
0
5
10
15
20
25
30
35
40
45
50
55
60
65
70
75
80
85
90
95
100
RETURN FLOW DISCHARGE (ml/sec)

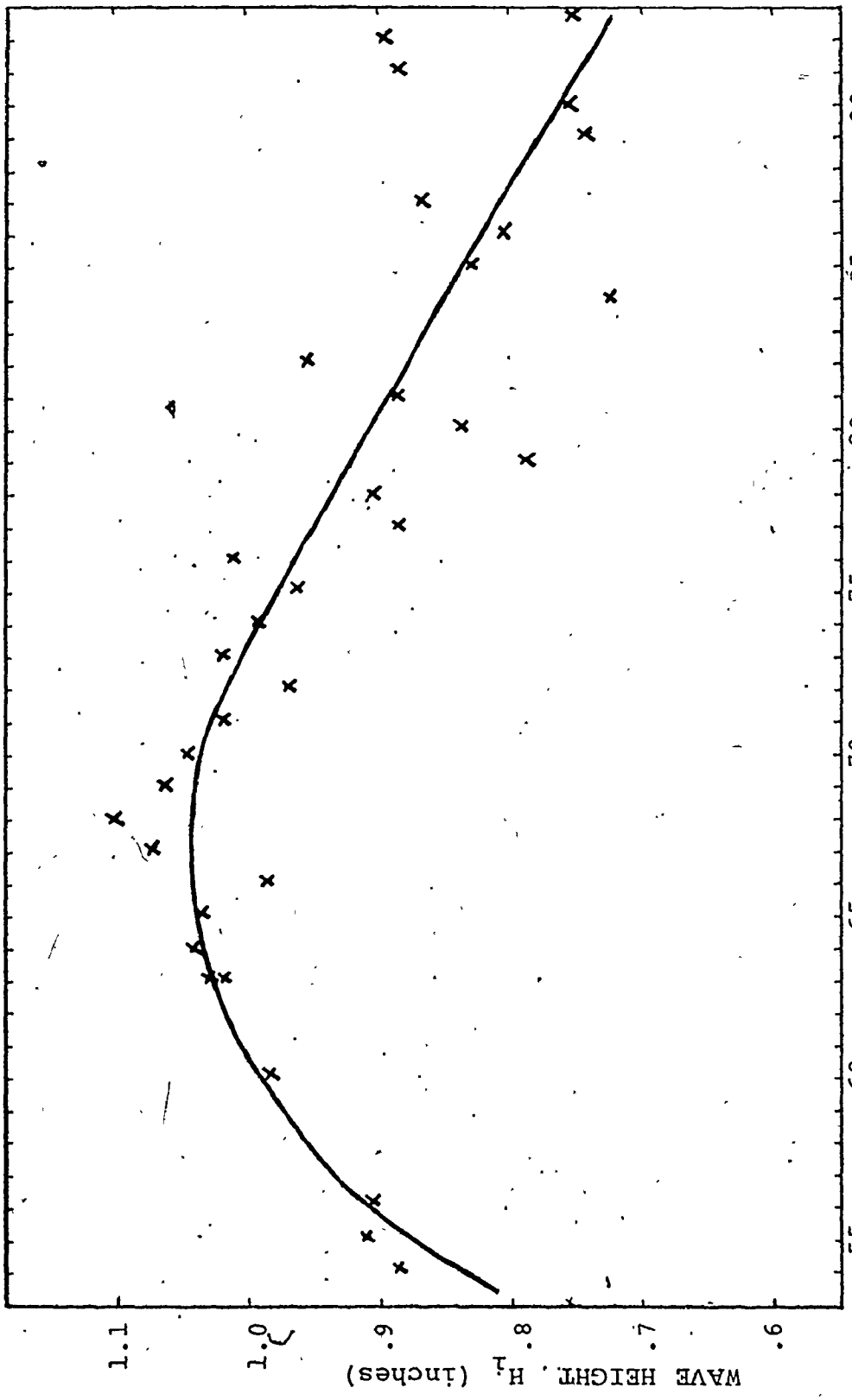
WAVE HEIGHT, H_i (inches)
1.1
1.0
.9
.8
.7
.6
WAVE PERIOD T
.55
.60
.65
.70
.75
.80
.85
.90